

Strength of statistical evidence for genuine tripartite nonlocality

Soumyadip Patra and Peter Bierhorst

Department of Mathematics, University of New Orleans, New Orleans, Louisiana 70148, USA

(Dated: July 30, 2024)

Recent advancements in network nonlocality have led to the concept of local operations and shared randomness-based genuine multipartite nonlocality (LOSR-GMNL). In this paper, we consider two recent experimental demonstrations of LOSR-GMNL, focusing on a tripartite scenario where the goal is to exhibit correlations impossible in a network where each two-party subset shares bipartite resources and every party has access to unlimited shared randomness. Traditional statistical analyses measuring violations of witnessing inequalities by the number of experimental standard deviations do not account for subtleties such as memory effects. We demonstrate a more sound method based on the prediction-based ratio (PBR) protocol to analyse finite experimental data and quantify the strength of evidence in favour of genuine tripartite nonlocality in terms of a valid p -value. In our work, we propose an efficient modification of the test factor optimisation using an approximating polytope approach. By justifying a further restriction to a smaller polytope we enhance practical feasibility while maintaining statistical rigour.

I. INTRODUCTION

The standard bipartite Bell scenario, where two spatially separated parties perform local measurements on an entangled system, has been pivotal in demonstrating quantum correlations that defy any local hidden variable explanation [1–4]. Over the past decade, loophole-free experimental demonstrations of such correlations have not only ruled out classical descriptions of Nature [5–9] but have also enabled tasks such as device-independent quantum key distribution [10–12] and device-independent quantum random number generation [13–16].

The standard notion of Bell nonlocality is insufficient for addressing genuine nonlocality in scenarios involving more than two parties. In a tripartite scenario, according to previously held notions of genuine multipartite nonlocality (GMNL) [17, 18], correlations are considered genuinely multipartite nonlocal if their nonlocality cannot be reduced to bipartite nonlocality; that is, if they cannot be decomposed into convex combinations of exclusively bipartite-nonlocal correlations.

Over the past decade, nonlocality in network scenarios has been extensively researched [19–22] leading to a new definition, referred to as LOSR-GMNL, based on the framework of local operations and shared randomness (LOSR) [23, 24], which substituted the previously held notion [25] based on local operations and classical communication (LOCC) [26]. In a tripartite scenario, the new definition can be understood as follows: Consider three spatially separated parties where every two-party subset shares bipartite resources, which may include classical randomness, copies of maximally entangled quantum states, or super-quantum resources like the paradigmatic Popescu-Rohrlich (PR) Box [27]. The parties perform local operations on their portions of the resources they share and have access to unbounded shared local randomness. Correlations inexplicable in such a strategy exhibit LOSR-GMNL.

Recently, genuinely tripartite nonlocal correlations

have been experimentally claimed in [28–30]. In [28, 29], employing the techniques developed in [21, 31], the authors obtain novel Bell-type inequalities satisfied by tripartite correlations permissible in a strategy based on local operations on bipartite resources supplemented with globally shared local randomness, but violated by appropriate measurements on three-way entangled Greenberger-Horne-Zeilinger (GHZ) states. Then these linear inequalities' violations serve as device-independent (DI) witnesses for genuine tripartite nonlocality (GTNL). Using estimated measurement-settings-conditional outcome probabilities from a large number of experimental trials implementing a photonic tripartite GHZ protocol, both [28] and [29] claim GTNL by reporting the degree of violation of the DI witnesses in terms of the number of standard deviations (SDs) beyond their maximal value. Both works report a large number of experimental SDs of violation of their respective DI witness.

Although the high degree of violation in terms of the number of SDs reflects the precision with which the DI witnesses are violated, it is not a valid quantification of the strength of statistical evidence for GTNL. This approach fails to properly quantify the probability that, due to statistical fluctuations in a finite number of trials, the DI witnesses could be violated by distributions that still admit an explanation in terms of bipartite resources and shared randomness. Moreover, the method does not account for the potential for a memory attack to have influenced the experimental results [32]. In experiments with a fixed number of trials, the results of a given trial could depend on those from previous trials, especially if the prepared tripartite state and/or measurement settings vary arbitrarily over time.

In this paper, we present a robust method for statistical analysis of experimental data, and quantify the strength of evidence for GTNL. Our method is based on the prediction-based ratio (PBR) protocol, proposed in [33, 34], where the authors analyse data from Bell-test experiments demonstrating a departure from local realism, and quantify the evidence of departure in terms

of a valid p -value. Other than the test of local realism and demonstration of GTNL, the PBR protocol is also applicable in statistical analysis of finite data demonstrating other properties such as entanglement detection [35, 36], quantification of entanglement [37–39], Hilbert space dimension [40], and fidelity to some target state [41, 42] that involve violating DI linear witnesses such as Bell-type inequalities [43]; furthermore, the PBR protocol is also closely related to probability estimation factors (PEFs) involved in the framework of probability estimation—used in certifying device independent quantum randomness upon finite data obtained from loophole-free Bell experiments [44–46]. The PBR method allows the possibility that the outcomes in a given trial are dependent on the outcomes and measurement settings of the previous trials, hence the analysis is not subject to the memory loophole. It remains valid in presence of state fluctuations over time, variations in measurement settings and other experimental parameters such as detector efficiency, and is asymptotically optimal [33].

In our work, we consider count data from the experimental demonstrations in [28, 29]. After implementing a maximum-likelihood-based optimisation procedure to mitigate the presence of weak signalling effects usually present in finite experimental data, we use the derived empirical trial distribution to obtain valid p -values quantifying the evidence in favour of GTNL, where the p -value is calculated based on a *test statistic* which is a function of the data actually observed in the experiment. The test statistic employed in our work is a trialwise multiplicative accumulation of non-negative real-valued functions of the trial results, which we refer to as *test factors*. The PBR method uses a heuristic-based optimisation routine to find useful test factors by maximising the expected base-2 logarithm of the test factor with respect to the maximum-likelihood no-signalling estimate of the empirical trial distribution, subject to the constraint that the expected value of the test factor is at most one for distributions achievable with bipartite resources and shared randomness.

Since characterising the set of such distributions remains a challenging problem and the test factor optimisation requires a finite number of constraints, we employ a modification by considering an approximating polytope containing such distributions, obtained from a vertex enumeration routine for the intersection of the tripartite no-signalling polytope (for binary settings and outcomes) and the DI witness. The method of using an approximating polytope for an otherwise hard-to-characterise set has previously been used in the related context of probability estimation [44, 45, 47]. A key new aspect of our work is that we are then able to reduce the computation overload by considering instead the polytope comprising no-signalling distributions that saturate the DI witness instead of obeying it, replacing an inequality constraint with an equality constraint, which we justify rigorously. Consequently, we achieved a reduction in the number of optimisation constraints by an order of magnitude. Our

reduction technique can be applied to PBR-based statistical analysis for other properties detected by DI linear witnesses, including entanglement detection, Hilbert space dimension, fidelity to a pure state, and probability estimation. This promises to be an important reduction technique as network experiments of increasing numbers of parties, measurement settings, and outcomes require consideration of distribution polytopes of much increased dimension and complexity.

In the next sections, we discuss the specific DI linear witnesses used in [28, 29] as signatures for GTNL, the test factor method to quantify the evidence for GTNL, and the analysis of count data from the two experimental demonstrations.

II. BELL-TYPE TEST FOR GTNL

We study a scenario involving three space-like separated parties A, B, C with respective measurement settings labelled in binary as $x, y, z \in \{0, 1\}$, where for each measurement, they observe one out of two possible outcomes also labelled in binary as $a, b, c \in \{0, 1\}$. We refer to the settings-conditional outcome probabilities $P(abc|xyz)$ as *behaviours* and, to have a geometric formulation, denote them as vectors $\mathbf{P} \in \mathbb{R}^{64}$, whose components are the $2^6 = 64$ probabilities $P(abc|xyz)$ of the settings-outcome combinations. The parties are constrained by the relativistic principle of no instantaneous-signalling which means that the behaviours satisfy the no-signalling conditions (see Appendix A for a short review of the no-signalling set).

Figure 1 shows a network of three parties where each subset of two parties shares a (possibly super-quantum) bipartite-nonlocal resource and each party performs local operations on its portion of the bipartite resource shared with the other parties. Additionally, the parties have access to shared local randomness. Bell-type inequalities proposed in [28] and [29] are obeyed by all behaviours induced by a Figure 1-style network; behaviours violating these inequalities require three-way nonlocal resources and thus are considered genuinely tripartite nonlocal. In this sense, the inequalities are DI witnesses for GTNL. Both witnesses are obtained theory-agnostically using the inflation techniques developed in [21, 31] under the assumption of compatibility with device replication and a causal structure that includes classical, quantum and generalised probabilistic theories. The witnesses are as shown below:

$$\mathcal{M}_{AB}^{00} + \mathcal{M}_{AB}^{01} + \mathcal{C}_{ABC}^{101} - \mathcal{C}_{ABC}^{111} + 2\mathcal{M}_{AC}^{00} \leq 4, \quad (1)$$

$$\begin{aligned} \mathcal{M}_{AB}^{00} - \mathcal{M}_{AB}^{01} + \mathcal{M}_{BC}^{00} - \mathcal{M}_{BC}^{10} + 2\mathcal{C}_{ABC}^{101} \\ + 2\mathcal{C}_{ABC}^{111} + 4\mathcal{M}_{AC}^{00} \leq 8, \end{aligned} \quad (2)$$

where the marginal correlators (\mathcal{M}_A^x , \mathcal{M}_{AB}^{xy} , and likewise)

and full correlators (\mathcal{C}_{ABC}^{xyz}) are as defined as:

$$\mathcal{M}_A^x := \sum_a (-1)^a P(a|x) \quad (3)$$

$$\mathcal{M}_{AB}^{xy} := \sum_{a,b} (-1)^{a+b} P(ab|xy) \quad (4)$$

$$\mathcal{C}_{ABC}^{xyz} := \sum_{a,b,c} (-1)^{a+b+c} P(abc|xyz). \quad (5)$$

Interestingly, the witness in (2) can be derived from that in (1), as demonstrated in [48], by adding together two relabelled versions of (1). However, as pointed out in [48] that since the two relabelled versions of (1) are each linear witnesses themselves, i.e., their violation requires genuinely tripartite nonlocal behaviours, their sum which is (2) is not necessarily a weaker witness of GTNL than (1). In fact, in section IV we infer that it is the contrary for a specific case involving the depolarised GHZ behaviour. The fact that the two witnesses are inequivalent, even though one is derivable from the other, will be more evident later in section IV where we compare the two polytopes obtained by the intersection of the no-signalling set with the corresponding linear witnesses for our data analyses.

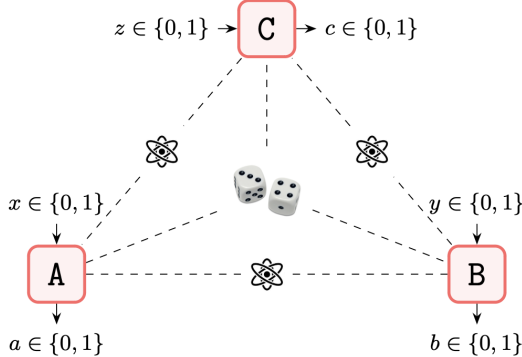


FIG. 1. Only behaviours impermissible under a strategy depicted above, involving local operations on (possibly generalised) bipartite nonlocal resources supplemented with unlimited shared randomness, are considered genuinely tripartite nonlocal. The photon symbols shared by every subset of two parties denote the shared bipartite resource. The three-way shared dice represent globally shared local randomness.

The maximum quantum violations, $2 + 2\sqrt{2}$ and $4 + 4\sqrt{2}$ for witnesses (1) and (2), respectively, are achieved by behaviours realisable in a protocol involving the pure state $|\text{GHZ}\rangle = \frac{1}{\sqrt{2}}(|000\rangle + |111\rangle)$ shared by the three parties where each party performs localised projective measurements $\mathbf{r} \cdot \boldsymbol{\sigma}$ in suitable directions $\mathbf{r} \in \mathbb{S}^2$ (see the ideal protocol described in [28] and [29] for the directions). The vector $\boldsymbol{\sigma} \equiv (X, Y, Z)$ represents the vector of 2×2 Pauli matrices. Using the linear relations in (A5) we can express the inequalities in (1) and (2) as

$$\sum_{a,b,c,x,y,z} B(abcxyz)P(abc|xyz) \leq \beta,$$

which we abbreviate using a geometric formulation as $\mathbf{B} \cdot \mathbf{P} \leq \beta$, where $\mathbf{B} \in \mathbb{R}^{64}$ is a Bell vector of the $B(abcxyz)$ coefficients. Note the marginal correlators appearing in the DI witnesses in (1) and (2) are well-defined due to the no-signalling conditions, depending only on the measurement settings of the parties involved. For instance, $\mathcal{M}_A^x = \mathcal{M}_A^{xyz}$ and $\mathcal{M}_{AB}^{xy} = \mathcal{M}_{AB}^{xyz}$. Consequently, the Bell vectors corresponding to the witnesses are not unique. Tables XIII and XIV in Appendix C show two possible Bell vectors for the witnesses, $\mathbf{B}_{(1)}$ for (1) and $\mathbf{B}_{(2)}$ for (2).

III. STRENGTH OF STATISTICAL EVIDENCE USING TEST FACTORS

An experiment demonstrating GTNL consists of a number of trials. Each trial is associated with outcomes and measurement settings collectively referred to as the trial results. The trial results are modelled as a random tuple $(A_k, B_k, C_k, X_k, Y_k, Z_k)$ with $k \in [n]$. The *experiment results* are then denoted by the sequence of tuples $\{(A_k, B_k, C_k, X_k, Y_k, Z_k)\}_{k=1}^n$, where n is the number of trials. We are interested in quantifying the strength of statistical evidence, by means of a *p*-value, against the hypothesis $\mathcal{H}_{\text{lo2sr}}$ described as follows: *The trial results follow a distribution permissible within a strategy encompassing local operations on (possibly generalised) bipartite-nonlocal resources and unlimited shared local randomness.* Experiment results inconsistent with a behaviour satisfying (1) and (2) provide evidence against this hypothesis.

A *p*-value can be defined in association with a function T of the experiment results, referred to as a test statistic, as

$$p = \sup_{\text{lo2sr}} \text{Prob}[T(\mathbf{U}_{\text{lo2sr}}) \geq T(\mathbf{u})]. \quad (6)$$

In (6), $\mathbf{U}_{\text{lo2sr}}$ is a sequence U_1, U_2, \dots, U_n , where U_k is the random tuple $(A_k, B_k, C_k, X_k, Y_k, Z_k)$ following a distribution consistent with $\mathcal{H}_{\text{lo2sr}}$; the supremum is taken over all such distributions. The test statistic is composed of a product of non-negative functions of trial results $F(U_k)$ which we refer to as test factors and whose expected value is at most one for U_k distributed according to $\mathcal{H}_{\text{lo2sr}}$, so that test factors exceeding one on average suggest inconsistency with $\mathcal{H}_{\text{lo2sr}}$. The test factor F can in general be updated from trial to trial or from a batch of trials to another batch during run time [33], but for this work we consider a fixed function for all trials.

The test statistic is then defined as a trial-wise product of the test factors, i.e., $T(u_1, \dots, u_n) := \prod_{k=1}^n F(u_k)$. The following formula for $p_{(\text{PBR})}$ is a valid upper bound for the exact *p*-value (defined as the maximal probability that the test statistic is at least as extreme as the value actually observed from the data under the assumption

that the null hypothesis is true):

$$p_{(\text{PBR})} = \min \left\{ \left(\prod_{k=1}^n F(u_k) \right)^{-1}, 1 \right\}. \quad (7)$$

Validity of this p-value bound has been shown in [33] (refer to the arguments between (16) and (17) in section III C) where the null hypothesis is Local Realism, and can be adapted straightforwardly for the null hypothesis considered in our work, i.e., $\mathcal{H}_{\text{lo2sr}}$. Henceforth, we will refer to the upper bound in (7) to the exact p -value as a valid p -value.

Our method of obtaining useful test factors is to seek a high expected value of $\frac{1}{n} \log_2 T(U_1, \dots, U_n) = \frac{1}{n} \sum_{i=1}^n \log_2 F(U_i)$ [33]. Heuristically, in constructing the test factor F we assume a stable experiment with independent trials, where future results will be identically distributed according to an estimate of the true distribution typically derived from a reserved portion of the data from previous trials. Now, whether or not such assumptions are actually met only affects the quality of the p -value, not its validity. For the remainder of this paper a trial distribution $\mathbb{P} := \{P(abc|xyz)S(xyz)\}$ is associated with a trial behaviour \mathbf{P} assuming a known and fixed settings distribution $\{S(xyz)\}$; hence the term *distribution* in this context refers to unconditional joint probability distribution of trials which can be obtained from the associated *behaviour* (settings-condition outcome distribution) by multiplying by the settings distribution. We then perform the following optimisation to obtain useful TFs:

$$\begin{aligned} \max_F \quad & \mathbb{E}_{\mathbb{Q}}[\log_2 F(ABCXYZ)] \\ \text{subject to} \quad & \mathbb{E}_{\mathbb{P}}[F(ABCXYZ)] \leq 1, \forall \mathbf{P} \in \Delta_{\text{lo2sr}}, \\ & F(abcxyz) \geq 0, \forall a, b, c, x, y, z, \end{aligned} \quad (8)$$

where \mathbb{Q} is the anticipated trial distribution assuming a stable experiment and Δ_{lo2sr} is the set of behaviours consistent with $\mathcal{H}_{\text{lo2sr}}$. The idea behind the objective function is that based on our heuristic, for large values of n , the difference between the observed value of $\frac{1}{n} \sum_{k=1}^n \log_2 F(U_k)$ and the expected value of $\log_2 F(U)$ will be greater or less than zero with roughly equal probability due to the central limit theorem. And so the test factor achieving the optimum value will tend to yield the largest observed product of test factors. The objective in (8) always returns a non-negative value as the test factor defined as $F(abcxyz) = 1, \forall a, b, c, x, y, z$, is valid and its logarithm has an expected value of zero for any distribution. A positive expected $\log_2 F_{\text{opt}}$ with respect to the anticipated distribution \mathbb{Q} , where F_{opt} is the optimal test factor according to the optimisation, can be expected if \mathbb{Q} is not consistent with $\mathcal{H}_{\text{lo2sr}}$.

The set Δ_{lo2sr} is convex—the allowance of globally shared randomness in the model ensures that convex mixtures of behaviours in Δ_{lo2sr} are again in Δ_{lo2sr} —and hence, linearity of expectation justifies restricting the constraint $\mathbb{E}_{\mathbb{P}}[F] \leq 1$ to the set of extreme points

of Δ_{lo2sr} , as this will imply it holds for all behaviours in the convex set. However, a complete characterisation of Δ_{lo2sr} in terms of its extreme points remains a challenging open question. Furthermore, it is possible that it has curved boundaries in some regions, which would imply a continuum of extreme points. The test factor method, on the other hand, requires a finite set of optimisation constraints for the problem to be computable, i.e., in (8) the set of behaviours \mathbf{P} for which $\mathbb{E}_{\mathbb{P}}[F] \leq 1$ holds, must be extreme points of a polytope containing Δ_{lo2sr} . In the forthcoming data analysis we demonstrate how we address this issue by making some modifications to the feasibility region of (8).

IV. DATA ANALYSIS

A. Experimental data from Mao et al [28]

First, we present the analysis of count data for the experimental demonstration in [28] obtained from [49]. An empirical trial distribution is derived from the experimental data as $f_{\text{emp}}(abcxyz) = \frac{N(abc|xyz)}{\sum_{abc} N(abc|xyz)} S(xyz)$, where $N(abc|xyz)$ represents the count of outcome combinations a, b, c given the setting combinations x, y, z , and $S(xyz)$ is the fixed settings distribution which we take to be uniform, i.e., $S(xyz) = 1/8, \forall x, y, z$. Due to statistical fluctuations the empirical distribution might not satisfy the no-signalling conditions exactly. We therefore begin by obtaining a maximum-likelihood no-signalling (MLNS) estimate $\hat{\mathbb{Q}}$ of the empirical trial distribution as described in Appendix B and subsection B 1. Next, using this estimate we perform the following test factor optimisation:

$$\begin{aligned} \max_F \quad & \mathbb{E}_{\hat{\mathbb{Q}}}[\log_2 F(ABCXYZ)] \\ \text{subject to} \quad & \mathbb{E}_{\mathbb{P}}[F(ABCXYZ)] \leq 1, \forall \mathbf{P} \in \text{Ext}(\Xi'_{(1)}), \\ & F(abcxyz) \geq 0, \forall a, b, c, x, y, z. \end{aligned} \quad (9)$$

Notice in (9) that the condition $\mathbb{E}_{\mathbb{P}}[F] \leq 1$ is with respect to distributions \mathbb{P} whose corresponding behaviours \mathbf{P} belong to $\text{Ext}(\Xi'_{(1)})$, a set different from Δ_{lo2sr} as appears in (8). As discussed in the paragraph following (8), this is because we need to replace Δ_{lo2sr} with an approximating polytope to make the optimisation computable. A suitable candidate would be the set $\Xi_{(1)} := \{\mathbf{P} \in \Xi_{\text{ns}} : \mathbf{B}_{(1)} \cdot \mathbf{P} \leq 4\}$, i.e., the set of behaviours belonging to the tripartite no-signalling polytope Ξ_{ns} (for binary inputs and outcomes) and satisfying the inequality in (1). This results in a polytope lying in a 26-dimensional affine subspace of the ambient space \mathbb{R}^{64} . Due to the linearity of expectation and convexity of $\Xi_{(1)}$ we can further restrict the condition $\mathbb{E}_{\mathbb{P}}[F] \leq 1$ to only those distributions \mathbb{P} whose corresponding behaviours \mathbf{P} are the extreme points of $\Xi_{(1)}$. We denote the set of extreme points of $\Xi_{(1)}$ by $\text{Ext}(\Xi_{(1)})$. Listing the extreme points, or *vertices*, of a polytope expressed as an intersection of finite

number of hyperplanes and closed half-spaces is known as the *Vertex Enumeration* problem (refer to Appendix C and Table XV for a summary of the vertex enumeration routines considered in this work). Now, the cardinality of $\text{Ext}(\Xi_{(1)})$ corresponds to the number of optimisation constraints in (9), and $|\text{Ext}(\Xi_{(1)})| = 56767$.

We were able to reduce this number of optimisation constraints from 56767 to 3200, thereby streamlining the computation due to a reduction of more than an order of magnitude, by replacing the set $\Xi_{(1)}$ with the 25-dimensional polytope described as $\Xi'_{(1)} := \{\mathbf{P} \in \Xi_{\text{ns}} : \mathbf{B}_{(1)} \cdot \mathbf{P} = 4\}$. This polytope contains behaviours belonging to Ξ_{ns} that saturate (1). The number of extreme points were found to be $|\text{Ext}(\Xi'_{(1)})| = 3200$. We justify this reduction by showing that if the optimisation over $\Xi'_{(1)}$ is performed for a $\hat{\mathbb{Q}}$ corresponding to a behaviour \mathbf{Q} for which $\mathbf{B}_{(1)} \cdot \mathbf{Q} > 4$ (and we would only be interested in running the optimisation in such a case), then the resulting optimising test factor F_{opt} will not just satisfy $E_{\mathbb{P}_{\text{sat}}}[F_{\text{opt}}] \leq 1$ for \mathbb{P}_{sat} whose corresponding (no-signalling) behaviour \mathbf{P}_{sat} saturates the witness in (1), but will also satisfy $E_{\mathbb{P}_{\text{less}}}[F_{\text{opt}}] \leq 1$ for all \mathbb{P}_{less} whose corresponding (no-signalling) behaviour \mathbf{P}_{less} strictly satisfies the same witness. This method of reducing the number of constraints in the test factor optimisation will be applicable more generally in scenarios where statistical evidence is sought against a theory (modelled as a null hypothesis, for instance, $\mathcal{H}_{\text{lo2sr}}$ in this work) by means of a test employing linear witnesses and the prediction-based ratio (PBR) method.

We now prove the implication as follows. Consider the schematic diagram shown in Figure 2. The irregular polygon represents the 26-dimensional polytope $\Xi_{(1)}$ and the line touching it is the (25-dimensional) Bell hyperplane $\mathbf{B}_{(1)} \cdot \mathbf{P} = 4$. No-signalling behaviours lying in the intersection of the hyperplane and $\Xi_{(1)}$ are the ones that saturate the inequality in (1). Next, consider a point \mathbf{P}_{less} strictly satisfying $\mathbf{B}_{(1)} \cdot \mathbf{P} \leq 4$, hence lying below the hyperplane, and the point \mathbf{Q} (corresponding to the distribution $\hat{\mathbb{Q}}$ in the objective function of (9)) strictly violating the inequality, hence lying above the hyperplane. The points are labelled in the diagram. The dashed line joining the two points represents all points expressible as the convex combination $\lambda\mathbf{Q} + (1 - \lambda)\mathbf{P}_{\text{less}}$ for $\lambda \in [0, 1]$. Because the points \mathbf{Q} and \mathbf{P}_{less} satisfy, respectively, $\mathbf{B}_{(1)} \cdot \mathbf{Q} > 4$ and $\mathbf{B}_{(1)} \cdot \mathbf{P}_{\text{less}} < 4$, there is some $\lambda \in (0, 1)$ for which $\mathbf{B}_{(1)} \cdot (\lambda\mathbf{Q} + (1 - \lambda)\mathbf{P}_{\text{less}}) = 4$, i.e., for that specific value of λ the point $\lambda\mathbf{Q} + (1 - \lambda)\mathbf{P}_{\text{less}}$ lies in the intersection of the Bell hyperplane and the polytope; let us denote this point as $\mathbf{P}_{\text{sat}} = \lambda\mathbf{Q} + (1 - \lambda)\mathbf{P}_{\text{less}}$. We have $E_{\mathbb{P}_{\text{sat}}}[F_{\text{opt}}] \leq 1$, as the optimisation was performed to enforce this constraint for such distributions. Then expressing \mathbf{P}_{less} in terms of \mathbf{P}_{sat} and \mathbf{Q} as $\mathbf{P}_{\text{less}} = \frac{1}{1 - \lambda}(\mathbf{P}_{\text{sat}} - \lambda\mathbf{Q})$ we can show that the condition $E_{\mathbb{P}_{\text{sat}}}[F_{\text{opt}}] \leq 1$ implies $E_{\mathbb{P}_{\text{less}}}[F_{\text{opt}}] \leq 1$ (\mathbb{P}_{less} and \mathbb{P}_{sat} are the distributions corresponding to the behaviours \mathbf{P}_{less} and \mathbf{P}_{sat}): By the linearity of expectation we have

$E_{\mathbb{P}_{\text{less}}}[F_{\text{opt}}] = \frac{1}{1 - \lambda} \left(E_{\mathbb{P}_{\text{sat}}}[F_{\text{opt}}] - \lambda E_{\hat{\mathbb{Q}}}[F_{\text{opt}}] \right)$. As noted in the discussion following (8), $E_{\hat{\mathbb{Q}}}[\log_2 F_{\text{opt}}] \geq 0$ will always hold. Then, as $\log_2(E_{\hat{\mathbb{Q}}}[F_{\text{opt}}]) \geq E_{\hat{\mathbb{Q}}}[\log_2 F_{\text{opt}}]$ holds (due to Jensen's inequality) we can conclude that $E_{\hat{\mathbb{Q}}}[F_{\text{opt}}] \geq 1$ which implies $-\lambda E_{\hat{\mathbb{Q}}}[F_{\text{opt}}] \leq -\lambda$. Going back to the expression $E_{\mathbb{P}_{\text{less}}}[F_{\text{opt}}] = \frac{1}{1 - \lambda} \left(E_{\mathbb{P}_{\text{sat}}}[F_{\text{opt}}] - \lambda E_{\hat{\mathbb{Q}}}[F_{\text{opt}}] \right)$, we then deduce that $E_{\mathbb{P}_{\text{less}}}[F_{\text{opt}}] \leq \frac{1}{1 - \lambda} (E_{\mathbb{P}_{\text{sat}}}[F_{\text{opt}}] - \lambda) \leq 1$. Therefore, it suffices to have the test factor optimisation constraint $E[F] \leq 1$ with respect to only those distributions whose associated behaviours belong to $\Xi'_{(1)}$.

Subsequently, performing the optimisation in (9) with respect to the MLNS estimate $\hat{\mathbb{Q}}$ shown in Table VI in Appendix B, we obtain the optimal value $E_{\hat{\mathbb{Q}}}[\log_2 F_{\text{opt}}] \approx 0.017984$. The optimal test factor F_{opt} is presented in Table I. The evidence in favour of GTNL is quantified by the *p*-value which can be computed using F_{opt} and the count data from the experiment, shown in V. From the formula given in (7) a valid *p*-value can be obtained by inverting the product $\prod_{k=1}^n F_{\text{opt}}(u_k)$, where u_k denotes the trial results $(a_k, b_k, c_k, x_k, y_k, z_k)$ for the k 'th trial. That is, we find the product (over all setting-outcome combinations) of $F_{\text{opt}}(u)$ raised to the power of the corresponding count $\text{ct}(u)$ obtained from the count data in Table V and invert it, as shown below:

$$p = \prod_u \left(F_{\text{opt}}(u)^{\text{ct}(u)} \right)^{-1} \approx 3.691 \times 10^{-71}.$$

The extremely small *p*-value for this count data, which we will also notice for the other data, is not surprising given that the experimental violation of 4.6674 ± 0.0323 of the witness in (1) reported in [28] is more than 20 standard deviations beyond the mean value of 4. Notice that the *p*-values obtained in practice will be worse than the ones we obtained in our work. This is because in practice a portion of experimental data is set aside for testing, and the optimal test factor F_{opt} obtained from the training data is used on the test data to calculate a *p*-value. The only data we had at our disposal was the count data for both the experimental demonstrations in [28] and [29], and we use F_{opt} on the same data to calculate a *p*-value from which we obtained it. A test statistic optimised for a data set and then retroactively applied to the same data will in general suggest overly optimistic statistical evidence. However, the *p*-value we obtained is a good rough estimate for what one can expect to find in practice.

A potential issue with analysing the raw count data from experiments demonstrating GTNL is the presence of zero frequencies for certain settings-outcomes combinations. When there are zero-valued entries in the empirical trial distribution, the PBR method may assign a zero value to the test factor score for the corresponding settings-outcome combinations. If these combinations occur in a subsequent trial, the product in the expression for $p_{(\text{PBR})}$ in (7) will be set to zero, which will result in $p_{(\text{PBR})}$ being set to 1, without any possibility for

TABLE I. Optimal test factor F_{opt} obtained from the optimisation in (9) with respect to the maximum-likelihood no-signalling estimate (VI) of the empirical trial distribution. We use uniform settings distribution $S(xyz) = 1/8, \forall x, y, z$.

		abc							
		000	001	010	011	100	101	110	111
xyz	000	1.0598122	0.6337174	0.8904132	0.1605416	0.1597108	0.8806786	0.6151026	1.0322941
	001	1.0603007	1.0545397	0.8396764	0.8350988	0.7859199	0.7957258	1.0224645	1.0334538
	010	1.0451923	0.6765703	0.8714717	0.211803	0.2503016	0.8985366	0.6925647	1.0497528
	011	1.0404143	1.0480199	0.7723418	0.7959361	0.8458675	0.8379063	1.0437713	1.0517986
	100	1.0331707	0.8675255	0.879014	1.0171452	1.0395271	0.8790457	0.875241	1.018536
	101	1.17889	0.6058302	0.64111	1.1488267	0.5833145	1.1724989	1.1376239	0.6436649
	110	1.0152896	0.8936919	0.8646207	1.0340698	1.0271972	0.9004357	0.8652325	1.0295178
	111	0.5669301	1.1381454	1.1593922	0.6326589	1.1442416	0.5532124	0.6660395	1.1409818

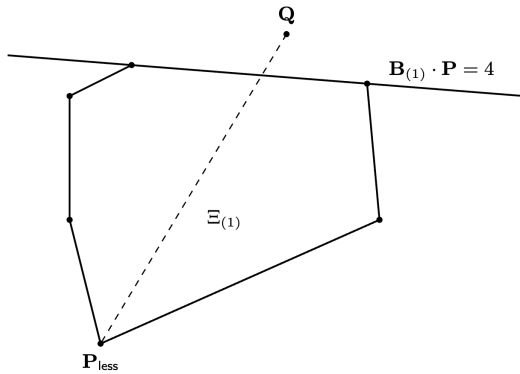


FIG. 2. A schematic diagram aiding in our proof for $E_{\mathbb{P}_{\text{sat}}}[F] \leq 1 \Rightarrow E_{\mathbb{P}_{\text{less}}}[F] \leq 1$. The irregular polygon represents the 26-dimensional polytope $\Xi(1)$ resulting from the intersection Ξ_{ns} and the halfspace $B(1) \cdot P \leq 4$. The points Q and P_{less} , respectively, violate and strictly satisfy the inequality $B(1) \cdot P \leq 4$. The portion of the hyperplane touching $\Xi(1)$ represent a 25-dimensional polytope. The point P_{sat} described in the main text is located at the intersection of the hyperplane and the dashed line.

later adjustment. Another count data set for the demonstration in [28] obtained from [49] that we analyse is as shown in Table VII where the derived three-party data has some instances of zero counts. The analysis for this data is same as before, except that after obtaining the MLNS estimate using the optimisation routine in (B1) with respect to the empirical trial distribution, we mix the estimate with some noise to address the zero count issue. Using this noise-mixed estimate we then perform the test factor optimisation. We explain these steps in more detail in Appendix B 1.

B. Experimental data from Cao et al [29]

Next, we analyse count data from the experimental demonstration in [29] (as reported in Table I in Appendix A), and reproduced here in Table X in Appendix B 2. The data in the table pertains to a four-party experiment from which we derive the relevant three-party data by following similar steps as in our previous analysis. During

this process, we encountered a missing data issue for two settings combinations, specifically $xyz \equiv 000, 010$. We addressed this problem by utilising existing data (refer to the row corresponding to the measurement combination ZZZX in Table X) from the original four-party experiment, along with a no-signalling argument. This allowed us to compute a MLNS estimate with a slight modification in the optimisation procedure; detailed explanations are provided in Appendix B 2.

The intersection of the polytope Ξ_{ns} with the witness (2) (equivalently, $B(2) \cdot P \leq 8$) results in the 26-dimensional polytope $\Xi(2)$, where $|\text{Ext}(\Xi(2))| = 57283$. Notice the difference in cardinality from our previous polytope ($|\text{Ext}(\Xi(1))| = 56767$) provides evidence that (1) cannot be derived from (2) through relabelling, which are symmetries of the no-signalling polytope, or through no-signalling adjustments to the inequalities. The 25-dimensional polytope $\Xi'(2)$ comprises no-signalling behaviours that saturate (2) (equivalently, satisfy $B(2) \cdot P = 8$), and $|\text{Ext}(\Xi'(2))| = 3664$. The restriction of the optimisation feasibility region by means of having the condition $E[F] \leq 1$ with respect to only those distributions whose corresponding behaviours belong to the set $\text{Ext}(\Xi'(2))$ is based on the same reasoning as in our previous data analysis.

After obtaining a MLNS estimate, we proceed to the test factor optimisation as shown below.

$$\begin{aligned}
 \max_F \quad & E_{\mathbb{Q}}[\log_2 F(ABCXYZ)] \\
 \text{subject to} \quad & E_{\mathbb{P}}[F(ABCXYZ)] \leq 1, \forall \mathbb{P} \in \text{Ext}(\Xi'(2)), \\
 & F(a0c000) = F(a1c000), \forall a, c, \\
 & F(a0c010) = F(a1c010), \forall a, c, \\
 & F(abxyz) \geq 0, \forall a, b, c, x, y, z.
 \end{aligned} \tag{10}$$

The optimal test factor F_{opt} obtained from (10) is presented in Table II. We introduce additional constraints to the optimisation routine in (10), specifically the TF “locking” constraints $F(a0cxyz) = F(a1cxyz)$ for all values of a, c and $xyz \equiv 000, 010$. This constraint results from our method of addressing the missing data problem. By enforcing these constraints we ensure that the test factors assign equal weight to the entries $F(a0cxyz)$ and $F(a1cxyz)$, which correspond to the entries $Q(a0cxyz)$

TABLE II. Optimal test factor F_{opt} obtained from the optimisation in (10) with respect to the maximum-likelihood no-signalling estimate (XII) of the empirical trial distribution. We use uniform settings distribution $S(xyz) = 1/8, \forall x, y, z$.

		abc							
		000	001	010	011	100	101	110	111
xyz	000	1.0073726	0.3733147	1.0073726	0.3733147	0.3679765	1.0122465	0.3679765	1.0122465
	001	1.0571756	1.0592063	0.745292	0.772362	0.7352839	0.7331479	1.0625527	1.0854559
	010	1.0073726	0.3733813	1.0073726	0.3733813	0.3679563	1.0122465	0.3679563	1.0122465
	011	0.7481449	0.7434019	1.0714002	1.0585814	1.0705442	1.069968	0.7546472	0.7459951
	100	1.0638622	0.7369682	0.7533695	1.0656278	1.0529862	0.7196825	0.7692114	1.0750601
	101	1.1853197	0.5666988	0.5293914	1.1640358	0.5684837	1.1670996	1.1641421	0.4594142
	110	0.7469697	1.0636082	1.0670628	0.744549	0.7476439	1.070692	1.0626543	0.7465501
	111	1.1837828	0.5268113	0.5404343	1.1698433	0.5325159	1.2149169	1.1725549	0.5847271

and $Q(a1cxyz)$ of the anticipated trial distribution for all values of a, c and $xyz \equiv 000, 010$. This is because, as discussed in Appendix B 2, in these cases only the sum $\sum_b Q(abcxyz)$ (and not the individual $Q(abcxyz)$ entries) can be considered to reflect the data of [29], and so we “lock” the test factors to not distinguish between the two $Q(abcxyz)$ for differing b .

We now compare the strengths of evidence against $\mathcal{H}_{\text{lo2sr}}$ for both experimental demonstrations in [28] and [29] with the strength of evidence for the distribution associated with a depolarised GHZ behaviour (assuming uniform settings distribution). The (perfect) GHZ behaviour maximally violating the witness in (2) results from the protocol shown in Figure 3. The protocol resulting in the GHZ behaviour that maximally violates the witness in (1) is same as that in Figure 3 with the only difference that party B measures $(Z - X)/\sqrt{2}$ for the setting choice $y = 1$. While the perfect GHZ behaviours from the

maximally entangled pure state $|\text{GHZ}\rangle$ with a depolarised GHZ state which we model in terms of the visibility parameter $\theta \in [0, 1]$ as $\Phi(\theta) = \theta |\text{GHZ}\rangle \langle \text{GHZ}| + (1 - \theta)I/8$ such that $\Phi(1)$ is the maximally entangled GHZ state and $\Phi(0)$ is the maximally mixed state $I/8$. The depolarised GHZ behaviour $\mathbf{P}_{\text{GHZ},\theta}$ resulting from the protocol shown in Figure 3 with $|\text{GHZ}\rangle$ replaced with $\Phi(\theta)$ is as presented in Table III. Similarly, we can obtain depolarised GHZ behaviour from the protocol (resulting in the perfect GHZ behaviour that maximally violates (1)) by replacing the state $|\text{GHZ}\rangle$ with $\Phi(\theta)$.

For visibility $\theta > 2/(\sqrt{2} + 1)$ the depolarised GHZ behaviour violates the witness in (2) (likewise for (1)). The red and blue curves in Figure 4 show a plot of the strength of evidence against $\mathcal{H}_{\text{lo2sr}}$ for the trial distributions $\mathbb{P}_{\text{GHZ},\theta} = \{P_{\text{GHZ},\theta}(abc|xyz)S(xyz)\}$, where $S(xyz) = 1/8, \forall x, y, z$, and $\mathbf{P}_{\text{GHZ},\theta}$ are the depolarised GHZ behaviours violating the respective inequalities in (1) and (2) for $\theta > 2/(\sqrt{2} + 1)$.

The horizontal lines (in red and blue) depict the strength of evidence for the MLNS estimate of the empirical trial distribution obtained from the experimental data in [28] and [29]. The red (respectively, blue) curve in Figure 4 is obtained by performing the optimisation in (10) (respectively, the one in (9)) for 120 equally spaced values of θ in the interval $(2/(\sqrt{2} + 1), 1]$ with $E_{\mathbb{P}_{\text{GHZ},\theta}}[\log_2 F]$ as the objective quantity to be maximised. The plot shows a monotonic increase in the strength of evidence for both depolarised GHZ distributions $\mathbb{P}_{\text{GHZ},\theta}$ as visibility θ increases beyond $2/(\sqrt{2} + 1)$.

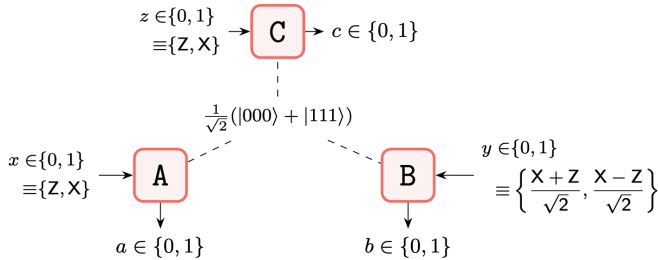


FIG. 3. An ideal protocol resulting in a (perfect) GHZ behaviour that achieves the maximal violation $4 + 4\sqrt{2}$ for the linear witness in (2). Parties A, C measure Z for $x, z = 0$ and measure X for $x, z = 1$, and party B measures $(X + Z)/\sqrt{2}$ for $y = 0$ and $(X - Z)/\sqrt{2}$ for $y = 1$. The choice of outcome labels $\{0, 1\}$ is up to convention and can be used interchangeably with $\{+1, -1\}$ (which is conventionally the set of outcomes for Pauli measurements).

ideal protocols maximally violate the (respective) linear witnesses in (1) and (2), thereby serving as a prototypical example of GTNL, practical considerations introduce noise, often modelled as a depolarising noise, as a result of which the pure state $|\text{GHZ}\rangle = \frac{1}{\sqrt{2}}(|000\rangle + |111\rangle)$ shared by the three parties is transformed into a mixed state. And so in the protocol displayed in Figure 3 we replace the

V. CONCLUSION

In this paper, we have demonstrated a robust statistical method for analysing data obtained from experiments demonstrating genuine tripartite nonlocality. We proposed a computationally efficient modification to the test factor optimisation using an approximating polytope approach. It resulted in a significant reduction in the number of optimisation constraints while ensuring statistical validity. This methodology not only enhances the reliability of detecting genuine tripartite nonlocality in finite data from experiments but can also be applied to tests

TABLE III. Depolarised GHZ behaviour resulting from the parties measuring a depolarised GHZ state $\Phi(\theta) = \theta |\text{GHZ}\rangle \langle \text{GHZ}| + (1 - \theta)I/8$ with visibility $\theta \in [0, 1]$. Parties A, C measure Z and X for $x, z = 0$ and $x, z = 1$, respectively, and party B measures $(X + Z)/\sqrt{2}$ for $y = 0$ and $(X - Z)/\sqrt{2}$ for $y = 1$. This behaviour violates (2) for visibility $\theta > \frac{2}{\sqrt{2}+1}$, and for $\theta = 1$ it is the perfect GHZ behaviour that achieves the maximum value of $4 + 4\sqrt{2}$ for the expression on the left hand side of (2).

		abc							
		000	001	010	011	100	101	110	111
xyz	000	$\frac{1+\theta+\sqrt{2}\theta}{8}$	$\frac{1-\theta}{8}$	$\frac{1+\theta-\sqrt{2}\theta}{8}$	$\frac{1-\theta}{8}$	$\frac{1-\theta}{8}$	$\frac{1+\theta-\sqrt{2}\theta}{8}$	$\frac{1-\theta}{8}$	$\frac{1+\theta+\sqrt{2}\theta}{8}$
	001	$\frac{2+\sqrt{2}\theta}{8}$	$\frac{2+\sqrt{2}\theta}{8}$	$\frac{2-\sqrt{2}\theta}{8}$	$\frac{2-\sqrt{2}\theta}{8}$	$\frac{2-\sqrt{2}\theta}{8}$	$\frac{2-\sqrt{2}\theta}{8}$	$\frac{2+\sqrt{2}\theta}{8}$	$\frac{2+\sqrt{2}\theta}{8}$
	010	$\frac{16}{1+\theta-\sqrt{2}\theta}$	$\frac{16}{1-\theta}$	$\frac{16}{1+\theta+\sqrt{2}\theta}$	$\frac{16}{1-\theta}$	$\frac{16}{8}$	$\frac{16}{1+\theta+\sqrt{2}\theta}$	$\frac{16}{8}$	$\frac{16}{1+\theta-\sqrt{2}\theta}$
	011	$\frac{8}{2-\sqrt{2}\theta}$	$\frac{16}{2-\sqrt{2}\theta}$	$\frac{16}{2+\sqrt{2}\theta}$	$\frac{16}{2+\sqrt{2}\theta}$	$\frac{16}{2+\sqrt{2}\theta}$	$\frac{16}{2+\sqrt{2}\theta}$	$\frac{16}{2-\sqrt{2}\theta}$	$\frac{16}{2-\sqrt{2}\theta}$
	100	$\frac{16}{2+\sqrt{2}\theta}$	$\frac{16}{2-\sqrt{2}\theta}$	$\frac{16}{2+\sqrt{2}\theta}$	$\frac{16}{2+\sqrt{2}\theta}$	$\frac{16}{2+\sqrt{2}\theta}$	$\frac{16}{2-\sqrt{2}\theta}$	$\frac{16}{2-\sqrt{2}\theta}$	$\frac{16}{2+\sqrt{2}\theta}$
	101	$\frac{16}{2+\sqrt{2}\theta}$	$\frac{16}{2-\sqrt{2}\theta}$	$\frac{16}{2-\sqrt{2}\theta}$	$\frac{16}{2+\sqrt{2}\theta}$	$\frac{16}{2-\sqrt{2}\theta}$	$\frac{16}{2+\sqrt{2}\theta}$	$\frac{16}{2+\sqrt{2}\theta}$	$\frac{16}{2-\sqrt{2}\theta}$
	110	$\frac{16}{2-\sqrt{2}\theta}$	$\frac{16}{2+\sqrt{2}\theta}$	$\frac{16}{2+\sqrt{2}\theta}$	$\frac{16}{2-\sqrt{2}\theta}$	$\frac{16}{2-\sqrt{2}\theta}$	$\frac{16}{2+\sqrt{2}\theta}$	$\frac{16}{2+\sqrt{2}\theta}$	$\frac{16}{2-\sqrt{2}\theta}$
	111	$\frac{16}{2+\sqrt{2}\theta}$	$\frac{16}{2-\sqrt{2}\theta}$	$\frac{16}{2-\sqrt{2}\theta}$	$\frac{16}{2+\sqrt{2}\theta}$	$\frac{16}{2-\sqrt{2}\theta}$	$\frac{16}{2+\sqrt{2}\theta}$	$\frac{16}{2+\sqrt{2}\theta}$	$\frac{16}{2-\sqrt{2}\theta}$

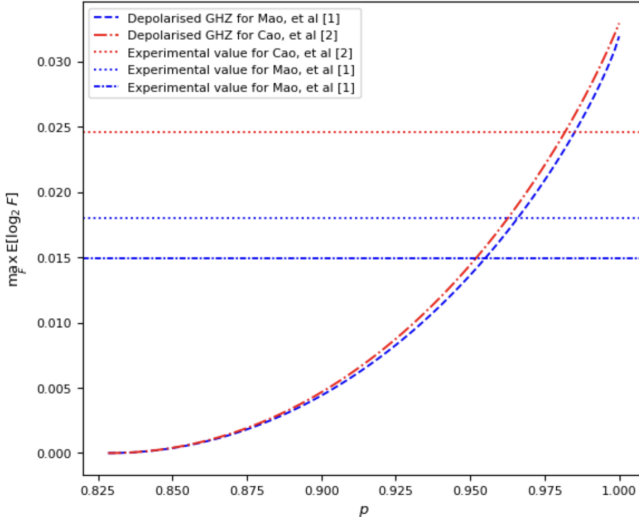


FIG. 4. Strength of evidence against $\mathcal{H}_{0,2s}$ for the trial distribution $\mathbb{P}_{\text{GHZ},\theta}$ associated with the depolarised GHZ behaviour $\mathbf{P}_{\text{GHZ},\theta}$ (assuming a uniform settings distribution) with visibility θ varying in the interval $(2/(\sqrt{2} + 1), 1]$: The red curve displays strength of evidence for $\mathbb{P}_{\text{GHZ},\theta}$ whose corresponding $\mathbf{P}_{\text{GHZ},\theta}$ (as displayed in Table III) violates the witness in (2) for $\theta > 2/(\sqrt{2} + 1)$. The blue curve displays strength of evidence for $\mathbb{P}_{\text{GHZ},\theta}$ whose corresponding $\mathbf{P}_{\text{GHZ},\theta}$ violates the witness in (1) for $\theta > 2/(\sqrt{2} + 1)$. The horizontal lines denote the strength of evidence demonstrated by the experimental data from [28] (shown in blue) and [29] (shown in red). The blue lines correspond to values of ≈ 0.014935 and ≈ 0.017984 and the red line corresponds to a value of ≈ 0.0245564 .

of properties involving violations of linear witnesses.

Besides [28, 29] another recent experimental demonstration of genuine tripartite nonlocality was reported in [30]. The tripartite scenario considered in this work is slightly different from the other two as party B has an extra setting, which makes it a $(2, 2; 2, 3; 2, 2)$ Bell scenario. More generally, the $(2, |\mathcal{X}|; 2, |\mathcal{Y}|; 2, |\mathcal{Z}|)$ Bell scenario is a tripartite scenario with three parties A, B, C with settings choices from the sets $\mathcal{X}, \mathcal{Y}, \mathcal{Z}$, respectively, where

each setting choice has two possible outcomes. We provide more details for the no-signalling set for this scenario in Appendix A. The DI witness used in [30] is

$$\text{CHSH}_{z=1}^{c=0} + \frac{4\text{Same} - 8}{1 + \mathcal{M}_C^1} \leq 2, \quad (11)$$

which is a combination of two Bell games: the CHSH game $\text{CHSH}_{z=1}^{c=0}$ between parties A and B conditioned on C obtaining the outcomes $c = 0$ for the measurement setting $z = 1$, and the “Same” game $\text{Same} := \mathcal{M}_{AB}^{02} + \mathcal{M}_{BC}^{20}$. We show in Appendix D that the witness in (11) is linear in that it can be expressed in the form $\mathbf{B} \cdot \mathbf{P} \leq \beta$ as shown in (D3). Thus, our method could be used to analyse the data in a similar way for [30], with the larger polytope defined by the no-signalling set and the witnessing inequality with the extra setting for party B. However, since this scenario is experimentally more difficult to implement with no known offsetting benefit (the simpler inequalities of (1) and (2) appear to be more noise resistant [28, 29]), future experiments do not seem likely to test this inequality.

It is important to note that the experiments performed in [28, 29] are subject to the locality loophole, and while the experiment in [30] ensured a space-like separation of the parties (thereby closing the locality loophole), all three experiments adopt a post-selection method in which they consider only those trials in which every party—each of which has two detectors—registers exactly one photon. Such experiments can only passively observe statistics consistent with a genuinely multipartite GHZ state in fundamentally limited fraction of trials—even if all components were improved to unit efficiency, there would always be multi-photon trials such that the non-post-selected statistics admit a model obeying the bipartite-only nonclassicality of Figure 1, or possibly even a fully classical model. (To illustrate, consider for example Figure 2a of [30] where the experimental setup is indeed consistent with Figure 1 as nonclassical resources comprise A-C and C-B bipartite quantum states; post-selection at C allows retro-inference of GHZ behaviour in a fraction of trials but the full data could never rule

out the Figure 1 model.) While the PBR protocol is valid in the presence of memory effects and statistical fluctuations in finite data from experiments, the method presented here does not formalise or otherwise account for extra assumptions required by an experiment employing post-selection—the data is analysed as though produced by a non-post-selected experiment. Future experiments employing space-like separation and generating high-quality GHZ states without post-selection, such as through heralding—and employing sound statistical analysis such as the method presented here—will be able to take the next steps towards definitively exhibiting the

phenomenon of genuine tripartite nonlocality.

ACKNOWLEDGMENTS

We thank Ya-Li Mao, Zheng-Da Li, Sixia Yu, and Jingyun Fan for sharing the count data from their experimental demonstration with us. This work was partially supported by NSF Grant No. 2328800 and AFOSR Grant No. FA9550-20-1-0067.

[1] J. S. Bell, On the Einstein-Podolsky-Rosen paradox, *Physics* **1**, 195 (1964).

[2] J. S. Bell, On the problem of hidden variables in quantum mechanics, *Rev. Mod. Phys.* **38**, 447 (1966).

[3] J. F. Clauser, M. A. Horne, A. Shimony, and R. A. Holt, Proposed experiment to test local hidden-variable theories, *Phys. Rev. Lett.* **23**, 880 (1969).

[4] N. Brunner, D. Cavalcanti, S. Pironio, V. Scarani, and S. Wehner, Bell nonlocality, *Rev. Mod. Phys.* **86**, 419 (2014).

[5] B. Hensen, H. Bernien, A. E. Dréau, A. Reiserer, N. Kalb, M. S. Blok, J. Ruitenberg, R. F. L. Vermeulen, R. N. Schouten, C. Abellán, W. Amaya, V. Pruneri, M. W. Mitchell, M. Markham, D. J. Twitchen, D. Elkouss, S. Wehner, T. H. Taminiau, and R. Hanson, Loophole-free Bell inequality violation using electron spins separated by 1.3 kilometres, *Nature* **526**, 682 (2015).

[6] M. Giustina, M. A. M. Versteegh, S. Wengerowsky, J. Handsteiner, A. Hochrainer, K. Phelan, F. Steinlechner, J. Kofler, J.-A. Larsson, C. Abellán, W. Amaya, V. Pruneri, M. W. Mitchell, J. Beyer, T. Gerrits, A. E. Lita, L. K. Shalm, S. W. Nam, T. Scheidl, R. Ursin, B. Wittmann, and A. Zeilinger, Significant-loophole-free test of Bell’s theorem with entangled photons, *Phys. Rev. Lett.* **115**, 250401 (2015).

[7] L. K. Shalm, E. Meyer-Scott, B. G. Christensen, P. Bierhorst, M. A. Wayne, M. J. Stevens, T. Gerrits, S. Glancy, D. R. Hamel, M. S. Allman, K. J. Coakley, S. D. Dyer, C. Hodge, A. E. Lita, V. B. Verma, C. Lambrocco, E. Tortorici, A. L. Migdall, Y. Zhang, D. R. Kumor, W. H. Farr, F. Marsili, M. D. Shaw, J. A. Stern, C. Abellán, W. Amaya, V. Pruneri, T. Jennewein, M. W. Mitchell, P. G. Kwiat, J. C. Bienfang, R. P. Mirin, E. Knill, and S. W. Nam, Strong loophole-free test of local realism, *Phys. Rev. Lett.* **115**, 250402 (2015).

[8] W. Rosenfeld, D. Burchardt, R. Garthoff, K. Redeker, N. Ortegel, M. Rau, and H. Weinfurter, Event-ready Bell test using entangled atoms simultaneously closing detection and locality loopholes, *Phys. Rev. Lett.* **119**, 010402 (2017).

[9] M.-H. Li, C. Wu, Y. Zhang, W.-Z. Liu, B. Bai, Y. Liu, W. Zhang, Q. Zhao, H. Li, Z. Wang, L. You, W. J. Munro, J. Yin, J. Zhang, C.-Z. Peng, X. Ma, Q. Zhang, J. Fan, and J.-W. Pan, Test of local realism into the past without detection and locality loopholes, *Phys. Rev. Lett.* **121**, 080404 (2018).

[10] A. K. Ekert, Quantum cryptography based on Bell’s theorem, *Phys. Rev. Lett.* **67**, 661 (1991).

[11] A. Acín, N. Brunner, N. Gisin, S. Massar, S. Pironio, and V. Scarani, Device-independent security of quantum cryptography against collective attacks, *Phys. Rev. Lett.* **98**, 230501 (2007).

[12] S. Pironio, A. Acín, N. Brunner, N. Gisin, S. Massar, and V. Scarani, Device-independent quantum key distribution secure against collective attacks, *New Journal of Physics* **11**, 045021 (2009).

[13] S. Pironio, A. Acín, S. Massar, A. B. de la Giroday, D. N. Matsukevich, P. Maunz, S. Olmschenk, D. Hayes, L. Luo, T. A. Manning, and C. Monroe, Random numbers certified by Bell’s theorem, *Nature* **464**, 1021 (2010).

[14] P. Bierhorst, E. Knill, S. Glancy, Y. Zhang, A. Mink, S. Jordan, A. Rommal, Y.-K. Liu, B. Christensen, S. W. Nam, M. J. Stevens, and L. K. Shalm, Experimentally generated randomness certified by the impossibility of superluminal signals, *Nature* **556**, 223 (2018).

[15] Y. Liu, Q. Zhao, M.-H. Li, J.-Y. Guan, Y. Zhang, B. Bai, W. Zhang, W.-Z. Liu, C. Wu, X. Yuan, H. Li, W. J. Munro, Z. Wang, L. You, J. Zhang, X. Ma, J. Fan, Q. Zhang, and J.-W. Pan, Device-independent quantum random-number generation, *Nature* **562**, 548 (2018).

[16] L. K. Shalm, Y. Zhang, J. C. Bienfang, C. Schlager, M. J. Stevens, M. D. Mazurek, C. Abellán, W. Amaya, M. W. Mitchell, M. A. Alhejji, H. Fu, J. Ornstein, R. P. Mirin, S. W. Nam, and E. Knill, Device-independent randomness expansion with entangled photons, *Nature Physics* **17**, 452 (2021).

[17] G. Svetlichny, Distinguishing three-body from two-body nonseparability by a Bell-type inequality, *Phys. Rev. D* **35**, 3066 (1987).

[18] J.-D. Bancal, J. Barrett, N. Gisin, and S. Pironio, Definitions of multipartite nonlocality, *Phys. Rev. A* **88**, 014102 (2013).

[19] T. Fritz, Beyond Bell’s theorem: correlation scenarios, *New Journal of Physics* **14**, 103001 (2012).

[20] M.-O. Renou, E. Bäumer, S. Boreiri, N. Brunner, N. Gisin, and S. Beigi, Genuine quantum nonlocality in the triangle network, *Phys. Rev. Lett.* **123**, 140401 (2019).

[21] E. Wolfe, A. Pozas-Kerstjens, M. Grinberg, D. Rosset, A. Acín, and M. Navascués, Quantum inflation: A general approach to quantum causal compatibility, *Phys. Rev. X* **11**, 021043 (2021).

[22] A. Tavakoli, A. Pozas-Kerstjens, M.-X. Luo, and M.-O. Renou, Bell nonlocality in networks, *Reports on Progress in Physics* **85**, 056001 (2022).

[23] X. Coiteux-Roy, E. Wolfe, and M.-O. Renou, No bipartite-nonlocal causal theory can explain nature's correlations, *Phys. Rev. Lett.* **127**, 200401 (2021).

[24] X. Coiteux-Roy, E. Wolfe, and M.-O. Renou, Any physical theory of nature must be boundlessly multipartite nonlocal, *Phys. Rev. A* **104**, 052207 (2021).

[25] D. Schmid, T. C. Fraser, R. Kunjwal, A. B. Sainz, E. Wolfe, and R. W. Spekkens, Understanding the interplay of entanglement and nonlocality: motivating and developing a new branch of entanglement theory, *Quantum* **7**, 1194 (2023).

[26] E. Chitambar, D. Leung, L. Mančinska, M. Ozols, and A. Winter, Everything you always wanted to know about locc (but were afraid to ask), *Communications in Mathematical Physics* **328**, 303 (2014).

[27] S. Popescu and D. Rohrlich, Quantum nonlocality as an axiom, *Foundations of Physics* **24**, 379 (1994).

[28] Y.-L. Mao, Z.-D. Li, S. Yu, and J. Fan, Test of genuine multipartite nonlocality, *Phys. Rev. Lett.* **129**, 150401 (2022).

[29] H. Cao, M.-O. Renou, C. Zhang, G. Massé, X. Coiteux-Roy, B.-H. Liu, Y.-F. Huang, C.-F. Li, G.-C. Guo, and E. Wolfe, Experimental demonstration that no tripartite-nonlocal causal theory explains nature's correlations, *Phys. Rev. Lett.* **129**, 150402 (2022).

[30] L. Huang, X.-M. Gu, Y.-F. Jiang, D. Wu, B. Bai, M.-C. Chen, Q.-C. Sun, J. Zhang, S. Yu, Q. Zhang, C.-Y. Lu, and J.-W. Pan, Experimental demonstration of genuine tripartite nonlocality under strict locality conditions, *Phys. Rev. Lett.* **129**, 060401 (2022).

[31] E. Wolfe, R. W. Spekkens, and T. Fritz, The inflation technique for causal inference with latent variables, *Journal of Causal Inference* **7**, 20170020 (2019).

[32] J. Barrett, D. Collins, L. Hardy, A. Kent, and S. Popescu, Quantum nonlocality, Bell inequalities, and the memory loophole, *Phys. Rev. A* **66**, 042111 (2002).

[33] Y. Zhang, S. Glancy, and E. Knill, Asymptotically optimal data analysis for rejecting local realism, *Phys. Rev. A* **84**, 062118 (2011).

[34] Y. Zhang, S. Glancy, and E. Knill, Efficient quantification of experimental evidence against local realism, *Phys. Rev. A* **88**, 052119 (2013).

[35] M. Horodecki, P. Horodecki, and R. Horodecki, Separability of mixed states: necessary and sufficient conditions, *Physics Letters A* **223**, 1 (1996).

[36] B. M. Terhal, Bell inequalities and the separability criterion, *Physics Letters A* **271**, 319 (2000).

[37] G. Vidal and R. F. Werner, Computable measure of entanglement, *Phys. Rev. A* **65**, 032314 (2002).

[38] G. Tóth, T. Moroder, and O. Gühne, Evaluating convex roof entanglement measures, *Phys. Rev. Lett.* **114**, 160501 (2015).

[39] R. Arnon-Friedman and J.-D. Bancal, Device-independent certification of one-shot distillable entanglement, *New Journal of Physics* **21**, 033010 (2019).

[40] N. Brunner, S. Pironio, A. Acin, N. Gisin, A. A. Méthot, and V. Scarani, Testing the dimension of hilbert spaces, *Phys. Rev. Lett.* **100**, 210503 (2008).

[41] J.-D. Bancal, M. Navascués, V. Scarani, T. Vértesi, and T. H. Yang, Physical characterization of quantum devices from nonlocal correlations, *Phys. Rev. A* **91**, 022115 (2015).

[42] T. H. Yang, T. Vértesi, J.-D. Bancal, V. Scarani, and M. Navascués, Robust and versatile black-box certification of quantum devices, *Phys. Rev. Lett.* **113**, 040401 (2014).

[43] W.-G. Chang, K.-C. Chen, K.-S. Chen, S.-L. Chen, and Y.-C. Liang, Device-independent certification of desirable properties with a confidence interval (2024), arXiv:2401.06627 [quant-ph].

[44] Y. Zhang, E. Knill, and P. Bierhorst, Certifying quantum randomness by probability estimation, *Phys. Rev. A* **98**, 040304 (2018).

[45] E. Knill, Y. Zhang, and P. Bierhorst, Generation of quantum randomness by probability estimation with classical side information, *Phys. Rev. Res.* **2**, 033465 (2020).

[46] S. Patra and P. Bierhorst, Asymptotically optimal adversarial strategies for the probability estimation framework, *Entropy* **25**, 10.3390/e25091291 (2023).

[47] P. Bierhorst and Y. Zhang, Tsirelson polytopes and randomness generation, *New Journal of Physics* **22**, 083036 (2020).

[48] P. Bierhorst, Consistency and causality of interconnected nonsignaling resources (2024), arXiv:2405.18408 [quant-ph].

[49] Private communication with the authors of *Phys. Rev. Lett.* 129, 150401 (2024).

[50] S. Pironio, J.-D. Bancal, and V. Scarani, Extremal correlations of the tripartite no-signalling polytope, *Journal of Physics A: Mathematical and Theoretical* **44**, 065303 (2011).

[51] E. Gawrilow and M. Joswig, polymake: a framework for analyzing convex polytopes, in *Polytopes—Combinatorics and Computation*, edited by G. Kalai and G. M. Ziegler (Birkhäuser Basel, Basel, 2000) pp. 43–73.

[52] S. Pironio, *Aspects of quantum nonlocality*, Ph.D. thesis, Université Libre de Bruxelles (2004).

[53] J. Barrett, N. Linden, S. Massar, S. Pironio, S. Popescu, and D. Roberts, Nonlocal correlations as an information-theoretic resource, *Phys. Rev. A* **71**, 022101 (2005).

Appendix A: No-signalling set for the $(2, |\mathcal{X}|; 2, |\mathcal{Y}|; 2, |\mathcal{Z}|)$ Bell scenario

We present a brief review of the no-signalling set of behaviours for a slightly more general three-party scenario. The scenario where parties have binary settings choice, i.e., $\mathcal{X}, \mathcal{Y}, \mathcal{Z} = \{0, 1\}$ is then a special case. The $(2, |\mathcal{X}|; 2, |\mathcal{Y}|; 2, |\mathcal{Z}|)$ Bell scenario consists of three space-like separated parties A, B and C performing measurements with random and private input x, y and z chosen from their respective sets \mathcal{X}, \mathcal{Y} and \mathcal{Z} and observing binary outcomes $a, b, c \in \{0, 1\}$ for each measurement. The parties are bound by the no instantaneous-signalling principle, consistent with special relativity, which requires that A cannot signal to B or C (and cyclic permutations) together with the stronger condition

that A cannot signal to the composite system (B, C) (and cyclic permutations). It is expressed as the following equality constraints on the setting-conditional outcome probabilities $\mathbf{P} := \{P(abc|xyz)\}$:

$$\sum_a P(abc|xyz) = \sum_a P(abc|x'yz), \forall b, c, x, x', y, z \quad (A1)$$

$$\sum_b P(abc|xyz) = \sum_b P(abc|xy'z), \forall a, c, x, y, y', z \quad (A2)$$

$$\sum_c P(abc|xyz) = \sum_c P(abc|xyz'), \forall a, b, x, y, z, z'. \quad (A3)$$

Besides the above constraints, the behaviours satisfy the non-negativity and the normalisation constraints, expressed, respectively, as $P(abc|xyz) \geq 0, \forall a, b, c, x, y, z$ and $\sum_{abc} P(abc|xyz) = 1, \forall x, y, z$.

Notice that we do not require a separate expression for the condition that the composite system (A, B) cannot signal to C (and cyclic permutations) because it can be deduced from (A1) and (A2), as demonstrated in [53], which we show below for completeness.

$$\begin{aligned} \sum_{a,b} P(abc|xyz) &= \sum_{a,b} P(abc|x'yz), \forall c, x, x', y, z \\ &= \sum_{a,b} P(abc|xy'z), \forall c, x, x', y, y', z. \end{aligned} \quad (A4)$$

The $8|\mathcal{X}||\mathcal{Y}||\mathcal{Z}|$ inequalities given by the non-negativity constraints describe closed half-spaces. Equalities given by the $|\mathcal{X}||\mathcal{Y}||\mathcal{Z}|$ normalisation constraints and the $4[(|\mathcal{X}|-1)|\mathcal{Y}||\mathcal{Z}| + |\mathcal{X}|(|\mathcal{Y}|-1)|\mathcal{Z}| + |\mathcal{X}||\mathcal{Y}|(|\mathcal{Z}|-1)]$ no-signalling constraints describe hyperplanes. The intersection of the closed half-spaces and the hyperplanes gives the no-signalling polytope. The ambient space containing Ξ_{ns} is \mathbb{R}^t , where $t = 8|\mathcal{X}||\mathcal{Y}||\mathcal{Z}|$; however, it is known that after subtracting redundancies, Ξ_{ns} is contained in a lower-dimensional affine space, the dimension of which is $\dim(\Xi_{\text{ns}}) = (|\mathcal{X}|+1)(|\mathcal{Y}|+1)(|\mathcal{Z}|+1) - 1$ (see Theorem 3.1 in [52]). For the scenario where each party has binary input choices, i.e., $\mathcal{X}, \mathcal{Y}, \mathcal{Z} = \{0, 1\}$, the no-signalling set Ξ_{ns} lies in a 26-dimensional affine subspace of \mathbb{R}^{64} and consists of 53,856 extreme points, of which 64 are local deterministic and the remaining grouped under 45 equivalence classes (see [50] for a complete list of the representative behaviours for each equivalence class along with the number of distinct behaviours obtained by a relabelling of outcomes, settings and parties). The expressions as defined in (3)–(5) for the marginalised and the full correlators can equivalently be written as shown below:

$$\begin{bmatrix} 1 \\ \mathcal{M}_A^x \\ \mathcal{M}_B^y \\ \mathcal{M}_C^z \\ \mathcal{M}_{AB}^{xy} \\ \mathcal{M}_{BC}^{yz} \\ \mathcal{M}_{AC}^{xz} \\ \mathcal{C}_{ABC}^{xyz} \end{bmatrix} = \begin{bmatrix} 1 & 1 & 1 & 1 & 1 & 1 & 1 & 1 \\ 1 & 1 & 1 & 1 & -1 & -1 & -1 & -1 \\ 1 & 1 & -1 & -1 & 1 & 1 & -1 & -1 \\ 1 & -1 & 1 & -1 & 1 & -1 & 1 & -1 \\ 1 & 1 & -1 & -1 & -1 & -1 & 1 & 1 \\ 1 & -1 & -1 & 1 & 1 & -1 & -1 & 1 \\ 1 & -1 & 1 & -1 & -1 & 1 & -1 & 1 \\ 1 & -1 & -1 & 1 & -1 & 1 & 1 & -1 \end{bmatrix} \begin{bmatrix} P(000|xyz) \\ P(001|xyz) \\ P(010|xyz) \\ P(011|xyz) \\ P(100|xyz) \\ P(101|xyz) \\ P(110|xyz) \\ P(111|xyz) \end{bmatrix}. \quad (A5)$$

The following compact expression for behaviour $\{P(abc|xyz)\}$, as a parametrisation of the outcomes and correlators, is obtained from the inverse of (A5).

$$\begin{aligned} P(abc|xyz) &= \frac{1}{8} \left[1 + (-1)^a \mathcal{M}_A^x + (-1)^b \mathcal{M}_B^y + (-1)^c \mathcal{M}_C^z + (-1)^{a \oplus b} \mathcal{M}_{AB}^{xy} + (-1)^{b \oplus c} \mathcal{M}_{BC}^{yz} + \right. \\ &\quad \left. (-1)^{a \oplus c} \mathcal{M}_{AC}^{xz} + (-1)^{a \oplus b \oplus c} \mathcal{C}_{ABC}^{xyz} \right]. \end{aligned} \quad (A6)$$

Appendix B: Maximum-likelihood no-signalling (MLNS) estimate

In this section we present the relevant details on obtaining a maximum-likelihood no-signalling estimate of an empirical trial distribution which is derived from the raw experimental data as $f_{\text{emp}}(abcxyz) = \frac{N(abc|xyz)}{\sum_{abc} N(abc|xyz)} S(xyz)$, where $N(abc|xyz)$ represents the count of outcome combinations a, b, c given the measurement settings combinations x, y, z . Owing to statistical fluctuations, $\{f_{\text{emp}}(abcxyz)\}$ may not adhere to the no-signalling and measurement settings constraints, potentially exhibiting weak signalling effects. So we obtain an estimate of the trial distribution that

satisfies these constraints. One method to obtain such an estimate is based on maximum-likelihood as mentioned in [33] (refer to the paragraph immediately following (A2) in Section 2 of the appendix). Assuming n iid trials, the likelihood of the trial data with empirical frequencies $\{f_{\text{emp}}(abcxyz)\}$, given that the true distribution is $\mathbb{Q} := \{Q(abcxyz)\}$, is proportional to $\prod_{abcxyz} Q(abcxyz)^{n f_{\text{emp}}(abcxyz)}$. The base-2 logarithm of this (ignoring the constant factor n) is the objective quantity to be maximised as shown below:

$$\begin{aligned}
& \max_{\mathbb{Q}} \sum_{abcxyz} f_{\text{emp}}(abcxyz) \log_2 Q(abcxyz) \\
\text{subject to} \quad & \sum_a Q(abc|xyz) = \sum_a Q(abc|x'yz), \forall b, c, x, x', y, z \\
& \sum_b Q(abc|xyz) = \sum_b Q(abc|xy'z), \forall a, c, x, y, y', z \\
& \sum_c Q(abc|xyz) = \sum_c Q(abc|xyz'), \forall a, b, x, y, z, z' \\
& \sum_{a,b,c} Q(abcxyz) = S(xyz), \forall x, y, z. \tag{B1}
\end{aligned}$$

In (B1), the first three constraints represent the absence of signalling, followed by the requirement that \mathbb{Q} must conform to the settings distribution. The result obtained from (B1) is the maximum-likelihood no-signalling (MLNS) estimate $\hat{\mathbb{Q}}$ of the empirical trial distribution. Given the concavity of the objective function, the maximisation routine in (B1) can be implemented using a standard convex optimisation programme. It must be noted, however, that when implementing (B1) additional constraints pertaining to non-negativity must be included since the estimate $\hat{\mathbb{Q}}$ that we are seeking is a distribution of the experiment results. The optimisation routine to obtain useful TFs is then performed with respect to $\hat{\mathbb{Q}}$.

1. MLNS estimate for experimental data from [28]

For the experimental demonstration in [28] we obtained two different count datasets from the authors of that work [49]. We first consider the count dataset for a four-party GHZ experiment implementing a protocol involving the state $|\Phi\rangle = \frac{1}{\sqrt{2}}(|0000\rangle + |1111\rangle)$. The four-party data must be processed to obtain the three-party data. The data for a three-photon GHZ experiment is derived from a four-photon GHZ experiment by measuring the third photon in the X basis and conditioning on the “+” outcome [28, 49]. And so in Table IV we present only that portion of the four-party data from [49] where the third party’s measurement setting is X . Columns corresponding to outcome combinations where the third entry is a “-” are then ignored.

TABLE IV. Count data obtained from [49] for the four-party GHZ experiment performed in [28]. The columns labelled by the various combinations of $\{+, -\}$ denote the measurement outcomes and the rows denote the (Pauli) measurements. The empirical trial distribution is obtained from the three-party data processed from this four-party data, by ignoring the shaded columns where the third party observes “ $-$ ”

$++\perp\perp$	$++\perp+$	$++-\perp$	$++-\perp$	$+-\perp+$	$+-\perp-$	$+-\perp-$	$+-\perp-$	$-+\perp+$	$-+\perp+$	$-+\perp-$							
$z\frac{x+z}{\sqrt{2}}xz$	550	3	541	2	114	3	130	1	4	113	4	113	5	826	3	923	
$z\frac{x+z}{\sqrt{2}}xx$	257	282	306	312	64	67	69	78	51	51	52	67	485	466	460	426	
$z\frac{x-z}{\sqrt{2}}xz$	87	2	82	0	671	1	737	4	2	639	0	566	4	179	2	158	
$z\frac{x-z}{\sqrt{2}}xx$	45	64	55	61	373	365	391	355	309	322	290	295	81	73	72	91	
$x\frac{x+z}{\sqrt{2}}xz$	259	55	310	53	70	394	69	409	285	50	309	51	69	392	61	408	
$x\frac{x+z}{\sqrt{2}}xx$	275	63	57	302	104	401	393	86	54	293	252	57	434	94	74	411	
$x\frac{x-z}{\sqrt{2}}xz$	44	280	68	316	377	80	363	68	48	304	84	328	370	75	424	83	
$x\frac{x-z}{\sqrt{2}}xx$	280	58	60	298	68	373	363	72	73	329	302	67	354	59	103	396	

After this step, there is one more manipulation needed. In the original three-party protocol described in [28], party B performs the measurements $\frac{Z+X}{\sqrt{2}}$ and $\frac{Z-X}{\sqrt{2}}$. However, the four-party data we have from [49] uses the measurements $\frac{X+Z}{\sqrt{2}}$ and $\frac{X-Z}{\sqrt{2}}$ for the second photon. So for a given outcome combination of the first, third, and fourth photons, we swap the count entry where the outcome for the second photon is “+” with the count entry where the outcome for the second photon is “-”. Table V shows the empirical trial distribution obtained from the three-party count

data derived from the four-party data. In obtaining the empirical trial distribution, we have assumed a uniform measurement settings distribution $S(xyz) = 1/8, \forall x, y, z$.

TABLE V. Empirical trial distribution $f_{\text{emp}}(abcxyz)$ for the raw experimental data in Table IV assuming a uniform settings distribution $S(xyz) = 1/8, \forall x, y, z$.

		abc							
		000	001	010	011	100	101	110	111
xyz	000	0.04249073	0.00023177	0.00880717	0.00023177	0.00030902	0.00872991	0.00038628	0.06381335
	001	0.01864481	0.0204585	0.00464306	0.00486071	0.00369994	0.00369994	0.03518572	0.03380731
	010	0.05291798	0.00007886	0.0068612	0.00015773	0.00031546	0.01411672	0.00015773	0.05039432
	011	0.02856924	0.0279565	0.00344669	0.00490196	0.00620404	0.0055913	0.02366728	0.02466299
	100	0.02056861	0.00436785	0.00555909	0.03128971	0.02263342	0.00397078	0.00547967	0.03113088
	101	0.02000873	0.00458382	0.00756694	0.02917637	0.00392899	0.02131839	0.03157742	0.00683935
	110	0.02986375	0.00633714	0.00348542	0.02217997	0.02930925	0.00594106	0.00380228	0.02408112
	111	0.0053325	0.02925031	0.02195734	0.00454831	0.02776035	0.00462673	0.00572459	0.02579987

For the empirical trial distribution in Table V we use the maximisation routine in (B1) to find the MLNS estimate \hat{Q} . The optimisation routine in (9) is then performed with respect to the distribution in Table VI from which we obtain the optimal test factor given in Table I.

TABLE VI. MLNS estimate for the empirical distribution in Table V from the experiment in (1) conforming to the uniform settings distribution $S(xyz) = 1/8, \forall x, y, z$.

		abc							
		000	001	010	011	100	101	110	111
xyz	000	0.04600651	0.000163	0.01110175	0.00015666	0.00018501	0.00717552	0.00038714	0.05982447
	001	0.02213168	0.02403783	0.00572623	0.00553217	0.00357774	0.00378272	0.03074134	0.02947028
	010	0.05061083	0.00008486	0.00649748	0.00023468	0.00037697	0.0141965	0.00019509	0.05280355
	011	0.02510992	0.02558579	0.002747498	0.0039842	0.00775529	0.00681817	0.0265638	0.02643483
	100	0.02256865	0.00375386	0.00593747	0.02931907	0.02362281	0.00358466	0.00555143	0.03066206
	101	0.02153297	0.00478953	0.00709426	0.02816228	0.00417644	0.02303102	0.02937332	0.00684017
	110	0.0254654	0.00769418	0.00304072	0.02537874	0.0255224	0.0065872	0.00365184	0.02765951
	111	0.00514717	0.02801242	0.02348007	0.00493939	0.02771805	0.00439155	0.00583171	0.02547964

In [33], the authors address an issue of zero counts in raw data when testing local realism using the full-PBR protocol. In the presence of zero-valued counts in the raw count data, the empirical trial distribution obtained from it retains some zero-valued entries, in which case the PBR method may assign the value zero to the test factor score of the corresponding settings-outcome combinations. Then if the corresponding settings-outcome combinations occur in a subsequent trial, the p -value is set to 1 without any possibility for a later recovery. These zero counts result in zero frequencies for certain combinations of measurement settings and outcomes in the empirical distribution, adversely affecting the calculation of full-PBR p -values. We encounter this issue of zero counts in the second dataset obtained from [49]. The count data presented in Table VII is from the experiment in [28] implementing a protocol involving the state $|\Phi\rangle = \sqrt{\frac{1.5}{2}}|0000\rangle + \sqrt{\frac{0.5}{2}}|1111\rangle$, which is an unbalanced 4-qubit GHZ state. The three-party data derived from the four-party data retains some occurrences of zero counts; specifically, the entries for the settings-outcomes combinations $(++, -, Z \frac{X+Z}{\sqrt{2}} XZ)$, $(++, -, Z \frac{X-Z}{\sqrt{2}} XZ)$ and $(-, ++, Z \frac{X+Z}{\sqrt{2}} XZ)$. (The data processing steps to derive the three-party data is same as the previous dataset.) We then follow the approach outlined in [33] (refer to section 2 of the appendix) to deal with the issue of having zero frequencies in the empirical distribution obtained from the three-party data: we first use the optimisation routine in (B1) to obtain a first no-signalling estimate \hat{Q}_0 for the true distribution Q , with which we mix in a distribution that has no zero probabilities with a weight approaching zero as n grows. That is, the adjusted estimate \hat{Q}_1 is given as follows:

$$\hat{Q}_1(abcxyz) = \frac{n}{n+1}\hat{Q}_0(abcxyz) + \frac{1}{n+1}\frac{1}{8}S(xyz). \quad (\text{B2})$$

In (B2), we have mixed the first estimate \hat{Q}_0 with a distribution that, conditionally on the settings, is uniform and conforms to the settings distribution $S(xyz)$. In our implementations, we assume a uniform settings distribution, i.e., we substitute $S(xyz)$ with 1/8 for all x, y, z . The empirical distribution obtained from the three-party count data, which is derived from the four-party data shown in Table VII, is presented in Table VIII. The adjusted MLNS estimate, according to (B2), is presented in Table IX.

TABLE VII. Count data for the four-party GHZ experiment in [28] involving an unbalanced GHZ state. The columns and rows, respectively, denote the outcomes and measurements for the parties. To obtain the three-party data we ignore the columns in grey. The remaining data is used as is with the measurements (Z, X) corresponding to the settings choices (0, 1) for parties A and C and the measurements $\left(\frac{Z+X}{\sqrt{2}}, \frac{Z-X}{\sqrt{2}}\right)$ corresponding to the settings choices (0, 1) for party B.

	+++	++-	++-	++-	+-+	+-+	+-+	---	-+++	-+++	-+-	-+-	-+-	-+-	-+-	-+-
$Z\frac{X+Z}{\sqrt{2}}XZ$	204	0	282	1	73	2	69	0	0	24	2	18	2	138	0	155
$Z\frac{X+Z}{\sqrt{2}}XX$	110	111	136	133	27	37	50	31	10	11	7	5	85	75	70	69
$Z\frac{X-Z}{\sqrt{2}}XZ$	36	0	59	0	289	2	374	3	1	121	0	118	2	34	0	25
$Z\frac{X-Z}{\sqrt{2}}XX$	23	20	19	30	178	189	198	230	50	70	70	47	18	14	11	17
$X\frac{X+Z}{\sqrt{2}}XZ$	129	6	128	5	30	83	36	62	109	10	130	10	31	79	47	62
$X\frac{X+Z}{\sqrt{2}}XX$	125	51	36	126	7	112	101	7	56	119	133	39	111	11	6	137
$X\frac{X-Z}{\sqrt{2}}XZ$	12	61	21	55	150	11	183	11	22	50	19	48	171	7	205	11
$X\frac{X-Z}{\sqrt{2}}XX$	81	6	8	67	62	141	145	66	6	75	67	7	156	53	66	172

TABLE VIII. Empirical trial distribution for the raw experimental data in Table VII assuming a uniform settings distribution $S(xyz) = 1/8, \forall x, y, z$.

		abc							
		000	001	010	011	100	101	110	111
xyz	000	0.05756208	0.	0.02059819	0.00056433	0.	0.00677201	0.00056433	0.03893905
	001	0.02950644	0.02977468	0.00724249	0.00992489	0.0026824	0.00295064	0.02280043	0.02011803
	010	0.07448454	0.00051546	0.00927835	0.	0.00051546	0.00876289	0.00025773	0.03118557
	011	0.03959075	0.04203737	0.00511566	0.0044484	0.00400356	0.00311388	0.011121	0.0155694
	100	0.03380503	0.00157233	0.00786164	0.02175052	0.02856394	0.00262055	0.00812369	0.02070231
	101	0.02639358	0.01076858	0.00147804	0.02364865	0.01182432	0.02512669	0.0234375	0.00232264
	110	0.03873967	0.00284091	0.00309917	0.01575413	0.04416322	0.00180785	0.00568182	0.01291322
	111	0.01336207	0.03038793	0.0174569	0.0012931	0.03362069	0.01142241	0.0012931	0.01616379

TABLE IX. Adjusted MLNS estimate for the empirical trial distribution in Table VIII conforming to a uniform settings distribution. The estimate is obtained according to (B2), where \hat{Q}_0 is a first estimate obtained using (B1) with respect to Table VIII.

		abc							
		000	001	010	011	100	101	110	111
xyz	000	0.06625581	0.00000023	0.01811245	0.000047703	0.00001538	0.00495332	0.00062414	0.03456163
	001	0.03419785	0.03205819	0.00805397	0.01053551	0.00227225	0.00269645	0.01790048	0.01728529
	010	0.07628384	0.00046728	0.00808442	0.00000996	0.00046337	0.00806587	0.00017618	0.03144907
	011	0.0378644	0.03888672	0.00438742	0.00370697	0.00525107	0.00327817	0.01492167	0.01670358
	100	0.03348011	0.00208906	0.00817827	0.01873282	0.03279109	0.00286447	0.01055833	0.01630584
	101	0.02646714	0.00910203	0.00200123	0.02490986	0.01000296	0.02565261	0.02395322	0.00291095
	110	0.03841534	0.00460422	0.00324304	0.01621767	0.03833187	0.00392893	0.00501755	0.01524138
	111	0.01084723	0.03217232	0.01762114	0.00183957	0.03226824	0.00999257	0.00168794	0.01857098

2. MLNS estimate for the data from [29]

We now consider a count dataset from the experiment described in [29] involving a 4-photon GHZ state (refer to Table I in Appendix A of [29] for the count data). It is presented in this paper in Table X. Similar to the preceding subsection, we first process the four-photon data to obtain the three-party data. A three-photon GHZ state is obtained from a four-photon GHZ state by projecting the fourth party over the $|+\rangle$ basis and conditioning on the “+” outcome. And so in Table X, the data corresponding to only those measurement-outcome combinations in which the fourth photon is measured in a Pauli X with the resulting outcome “+” are retained. Also, for the rows in Table X involving the measurement $\frac{Z-X}{\sqrt{2}}$ for the second photon, for a given combination of outcomes for the first, third and fourth photon, we swap the entry for the outcome combination marked ‘+’ for the second photon with the entry for the outcome combination marked ‘-’ for the same photon. Again, this is necessary for the same reason as mentioned in the previous sub-section in B1. The original protocol in [29] has the measurements $\frac{X+Z}{\sqrt{2}}$ and $\frac{X-Z}{\sqrt{2}}$ for the second photon. However, in the count dataset from [29] the counts are reported for the measurements $\frac{Z+X}{\sqrt{2}}$ and $\frac{Z-X}{\sqrt{2}}$ for the second photon.

Next, we ignore the rows corresponding to the measurements XXXX, ZZZZ and ZZZX because they correspond to

settings combinations (for the first three parties) that do not belong to the original three-party protocol. In the original protocol parties A, C perform measurements (Z, X) for the settings choices (0, 1) and party B performs measurements $\left(\frac{X+Z}{\sqrt{2}}, \frac{X-Z}{\sqrt{2}}\right)$ for the settings choices (0, 1). For the remaining rows we see that they correspond to some (though not all) measurement settings combinations for the first three parties (after ignoring the fourth measurement X) that belong to the original three-party protocol. For instance, the first row in Table X with measurement combination $X\frac{Z+X}{\sqrt{2}}XX$ represents the settings combination 101, the second row represents 111, the third row represents 001 and so on. Finally, the entries shaded in grey and blue in Table X are not retained in the three-party count data.

Now, notice that we do not have count data for the settings combinations 000 and 010. If we revisit the linear witness in (2), all correlator terms (marginal as well as full) except \mathcal{M}_{AC}^{00} can be shown to depend on setting combinations that are directly available from the raw count data in Table X. Nonetheless, data relevant to \mathcal{M}_{AC}^{00} and the two missing settings combinations 000 and 010 is obtained from the row shaded in blue in Table X which represents the data for measurement combination ZZZX. According to the three-party protocol, while Z is a valid measurement for both A and C (as it represents the setting choice 0), it is not for party B. But using the linear relations in (A5) for the correlator \mathcal{M}_{AC}^{00} , we observe that it is expressible as shown below:

$$\mathcal{M}_{AC}^{00} = \sum_{a,b,c} (-1)^{a \oplus c} P(abc|0y0) = \sum_{a,c} (-1)^{a \oplus c} (P(a0c|0y0) + P(a1c|0y0)), \text{ for } y \in \{0, 1\}. \quad (B3)$$

The second equality in (B3) emphasises that, for any $y \in \{0, 1\}$, to find \mathcal{M}_{AC}^{00} we need only the sums $P(a0c|0y0) + P(a1c|0y0)$ for the different combinations of the outcomes $a, c \in \{0, 1\}$. By no-signalling, we can obtain these from the ‘‘sum counts’’ $N(s+t|ZZZX) + N(s-t|ZZZX)$ for the four fixed choices of $s, t \in \{+, -\}$ from Table X, where $N(\cdot|ZZZX)$ denote counts for the relevant outcome combinations. Since the authors of [29] use number of experimental standard deviations for the individual correlator terms (both full and marginal) in their statistical analysis, it is our understanding that the relevant ‘‘sum counts’’ for the row representing the measurement combination ZZZX sufficed for estimating the correlator \mathcal{M}_{AC}^{00} . However, for our statistical analysis we require a three-party empirical trial distribution from processing the four-party count data, and so the individual count entries for all outcome combinations for those measurement combinations of the first three parties that represent settings combinations 000 and 010 are required. Our method for dealing with this is as follows: if $\#(abc|000)$ and $\#(abc|010)$ represent the counts for various combinations of $a, b, c \in \{0, 1\}$ for the settings combinations 000 and 010, then we obtain the count data for these two settings combinations from the row in blue in Table X using the following relations:

$$\begin{aligned} \sum_b \#(0b0|000) &= \sum_b \#(0b0|010) = N(+++|ZZZX) + N(+--|ZZZX), \\ \sum_b \#(0b1|000) &= \sum_b \#(0b1|010) = N(+-+|ZZZX) + N(-+-|ZZZX), \\ \sum_b \#(1b0|000) &= \sum_b \#(1b0|010) = N(-+-+|ZZZX) + N(--++|ZZZX), \\ \sum_b \#(1b1|000) &= \sum_b \#(1b1|010) = N(-+-|ZZZX) + N(--+|ZZZX). \end{aligned} \quad (B4)$$

Consider the first equality in (B4). We arbitrarily choose values for $\#(000|000)$ and $\#(010|000)$ such that their sum is equal to $N(+++|ZZZX) + N(+--|ZZZX)$. We do likewise for $\#(000|010)$ and $\#(010|010)$. The same process is repeated for the other three equalities. Once we obtain the three-party count data, we find the corresponding empirical trial distribution which is shown in Table XI. Subsequent computations below are set up so as not to depend on the arbitrary partitioning of these sum quantities into two counts.

Next, we use the maximum-likelihood procedure to obtain a no-signalling estimate for the empirical trial distribution that conforms to the fixed and known settings distribution. However, as a consequence of the way we have handled the missing data issue, we modify the maximum-likelihood procedure in (B1) as follows: Let \mathcal{S} denote the settings combinations $\{0, 1\}^3 \setminus \{(0, 0, 0), (0, 1, 0)\}$. Assuming n iid trials, given that the true distribution is \mathbb{Q} , the likelihood of the trial data with empirical frequencies $\{f_{\text{emp}}(abcxyz)\}$ is proportional to the expression in (B5). Notice that for the settings combinations (x, y, z) belonging to the set $\mathcal{S}' = \{(0, 0, 0), (0, 1, 0)\}$ we consider the sum of the probabilities $\sum_b Q(abcxyz)$ and raise it to the power of the corresponding sum of the frequencies $n \sum_b f_{\text{emp}}(abcxyz)$ for all combinations of outcomes a, c . This is to ensure our maximum likelihood estimate \hat{Q} does not depend on our arbitrary choices of $f_{\text{emp}}(a0cxyz)$ and $f_{\text{emp}}(a1cxyz)$, chosen only to satisfy the condition that their sum aligns with

TABLE X. Count data from [29] (see Table I in Appendix A). The columns and rows represent the outcomes and measurements, respectively. The three-party count data is obtained by ignoring the rows with the measurements **XXXX**, **ZZZZ**, **ZZZX** and the columns with the outcomes having a ‘-’ in the fourth place from the left (shaded grey), followed by some other manipulations involving the blue-shaded row as explained in the subsection B 2.

	++++	+++-	+-+-	++--	+-++	+-+-	+-+-	-+++	-+--	-++-	-+--	-+-+	-+-+	-+-+	-+-	
$x \frac{z+x}{\sqrt{2}} xx$	439	72	84	414	67	516	412	69	94	374	402	74	433	83	43	389
$x \frac{z-x}{\sqrt{2}} xx$	62	372	376	73	400	77	71	413	356	59	79	371	67	454	354	65
$z \frac{z+x}{\sqrt{2}} xx$	390	371	395	336	78	78	81	66	53	69	71	56	364	372	351	371
$z \frac{z-x}{\sqrt{2}} xx$	369	366	411	384	87	70	75	97	67	59	56	53	351	367	337	359
XXXX	450	5	11	451	9	513	531	7	4	430	428	9	499	5	9	461
ZZZZ	8552	16	13	0	9	11	14	18	15	19	11	13	0	19	20	8311
ZZZX	5229	4651	7	6	19	22	20	24	19	21	28	20	11	10	4426	4861
$x \frac{z+x}{\sqrt{2}} zx$	403	406	72	83	73	71	412	427	443	429	74	66	68	81	438	422
$x \frac{z-x}{\sqrt{2}} zx$	422	443	85	66	66	62	424	400	415	420	76	82	62	71	394	422

TABLE XI. Empirical trial distribution $f_{\text{emp}}(abcxyz)$ for the count data in Table X assuming a uniform settings distribution. Some frequencies in the 000 and 010 rows are chosen arbitrarily though they must match the condition (B4) as discussed in the text.

		abc							
		000	001	010	011	100	101	110	111
xyz	000	0.03355877	0.00017932	0.03366124	0.00016651	0.00019213	0.0284481	0.00019213	0.0286018
	001	0.02734156	0.02769209	0.00546831	0.00567863	0.00371565	0.00497757	0.02551879	0.0246074
	010	0.03366124	0.00016651	0.03355877	0.00017932	0.00019213	0.0286018	0.00019213	0.0284481
	011	0.00620365	0.00534797	0.02631204	0.0293069	0.02502852	0.02403023	0.00477752	0.00399315
	100	0.02540343	0.00453858	0.00460161	0.02597075	0.02792486	0.00466465	0.00428643	0.02760968
	101	0.02779889	0.00531915	0.00424265	0.02608916	0.00595238	0.02545593	0.02741895	0.0027229
	110	0.00424383	0.02726337	0.02713477	0.00546553	0.00398663	0.02533436	0.02668467	0.00488683
	111	0.02832861	0.00502833	0.00439093	0.0266289	0.00474504	0.02507082	0.02521246	0.0055949

TABLE XII. The MLNS estimate for the empirical trial distribution in Table XI assuming a uniform settings distribution.

		abc							
		000	001	010	011	100	101	110	111
xyz	000	0.05526551	0.00003347	0.00981915	0.00036254	0.0002421	0.00877659	0.00006518	0.05043548
	001	0.02766765	0.02763136	0.00485753	0.00532414	0.00412317	0.00489547	0.02624344	0.02425723
	010	0.01004867	0.00034732	0.05503599	0.00004868	0.00005569	0.05011917	0.0002516	0.00909291
	011	0.00578076	0.0046152	0.02674442	0.02834029	0.02540394	0.02477091	0.00496266	0.0043818
	100	0.02719486	0.00457093	0.00523716	0.02580832	0.02831269	0.00423915	0.00464719	0.02498969
	101	0.02637421	0.00539159	0.0043694	0.02667608	0.0054166	0.02713524	0.02673157	0.0029053
	110	0.00527976	0.0257657	0.02715226	0.00461355	0.0048246	0.02470077	0.02813528	0.00452807
	111	0.02623523	0.00481023	0.00450838	0.02725743	0.00494948	0.02457589	0.0271987	0.00546465

the corresponding sum on the right-hand side of (B4).

$$\prod_{(x,y,z) \in \mathcal{S}} \prod_{a,b,c} Q(abcxyz)^{n f_{\text{emp}}(abcxyz)} \prod_{(x,y,z) \in \mathcal{S}'} \prod_{a,c} \left[\sum_b Q(abcxyz) \right]^{n \sum_b f_{\text{emp}}(abcxyz)} \quad (\text{B5})$$

We then maximise the expression obtained by taking the base-2 logarithm of (B5) (where we ignore the constant factor n) as shown below in (B6). The constraints of the maximisation involve the no-signalling conditions and conformity to the fixed settings distribution.

$$\begin{aligned}
\max_{\mathbb{Q}} \quad & \sum_{(x,y,z) \in \mathcal{S}} \sum_{a,b,c} f_{\text{emp}}(abcxyz) \log_2 Q(abcxyz) + \sum_{(x,y,z) \in \mathcal{S}'} \sum_{a,c} \sum_b f_{\text{emp}}(abcxyz) \log_2 \sum_b Q(abcxyz) \\
\text{subject to} \quad & \sum_a Q(abc|xyz) = \sum_a Q(abc|x'yz), \forall b, c, x, x', y, z \\
& \sum_b Q(abc|xyz) = \sum_b Q(abc|xy'z), \forall a, c, x, y, y', z \\
& \sum_c Q(abc|xyz) = \sum_c Q(abc|xyz'), \forall a, b, x, y, z, z' \\
& \sum_{a,b,c} Q(abcxyz) = S(xyz), \forall x, y, z.
\end{aligned} \tag{B6}$$

The objective quantity in (B6) is a concave function in \mathbb{Q} , the proof of which is shown below, and hence the routine can be implemented using any standard convex optimisation programme. While this procedure returns estimates for $Q(a0cxyz)$ and $Q(a1cxyz)$ for the missing settings 000 and 010, it is unclear to what degree these estimates can be considered to reflect the actually recorded data in the experiment (as opposed to the sum of these quantities whose relation to the data is more well motivated). Thus in the main text, we choose to constrain the test factors to map $a0cxyz$ and $a1cxyz$ counts the same way on these settings.

Proposition B.1. *For the set $\mathcal{S} := \{0, 1\}^3 \setminus \{(0, 0, 0), (0, 1, 0)\}$ and $a, b, c \in \{0, 1\}$ the functional defined as:*

$$G(\mathbb{Q}) := \sum_{(x,y,z) \in \mathcal{S}} \sum_{a,b,c} f_{\text{emp}}(abcxyz) \log_2 Q(abcxyz) + \sum_{(x,y,z) \in \mathcal{S}'} \sum_{a,c} \sum_b f_{\text{emp}}(abcxyz) \log_2 \sum_b Q(abcxyz)$$

is concave in $\mathbb{Q} := \{Q(abcxyz)\}$.

Proof. To prove concavity of $G(\mathbb{Q})$ we need to show that $G(\mathbb{Q}) \geq \lambda G(\mathbb{Q}') + (1 - \lambda) G(\mathbb{Q}'')$ whenever $\mathbb{Q} = \lambda \mathbb{Q}' + (1 - \lambda) \mathbb{Q}''$ for $0 \leq \lambda \leq 1$. In the expressions that follow, we use the concise notations $\sum_{\mathcal{S}}$ and $\sum_{\mathcal{S}'}$ to mean, respectively, the sum over the settings combinations (x, y, z) belonging to the sets \mathcal{S} and \mathcal{S}' . We then can use the concavity of \log and manipulation of sums to write

$$\begin{aligned}
& G(\lambda \mathbb{Q}' + (1 - \lambda) \mathbb{Q}'') \\
= & \sum_{\mathcal{S}} \sum_{a,b,c} f_{\text{emp}}(abcxyz) \log_2 [\lambda Q'(abcxyz) + (1 - \lambda) Q''(abcxyz)] + \\
& \sum_{\mathcal{S}'} \sum_{a,c} \sum_b f_{\text{emp}}(abcxyz) \log_2 [\lambda \sum_b Q'(abcxyz) + (1 - \lambda) \sum_b Q''(abcxyz)] \\
\geq & \sum_{\mathcal{S}} \sum_{a,b,c} f_{\text{emp}}(abcxyz) [\lambda \log_2 Q'(abcxyz) + (1 - \lambda) \log_2 Q''(abcxyz)] + \\
& \sum_{\mathcal{S}'} \sum_{a,c} \sum_b f_{\text{emp}}(abcxyz) [\lambda \log_2 \sum_b Q'(abcxyz) + (1 - \lambda) \log_2 \sum_b Q''(abcxyz)] \\
= & \lambda \left(\sum_{\mathcal{S}} \sum_{a,b,c} f_{\text{emp}}(abcxyz) \log_2 Q'(abcxyz) + \sum_{\mathcal{S}'} \sum_{a,c} \sum_b f_{\text{emp}}(abcxyz) \log_2 \sum_b Q'(abcxyz) \right) \\
& + (1 - \lambda) \left(\sum_{\mathcal{S}} \sum_{a,b,c} f_{\text{emp}}(abcxyz) \log_2 Q''(abcxyz) + \sum_{\mathcal{S}'} \sum_{a,c} \sum_b f_{\text{emp}}(abcxyz) \log_2 \sum_b Q''(abcxyz) \right) \\
= & \lambda G(\mathbb{Q}') + (1 - \lambda) G(\mathbb{Q}'').
\end{aligned}$$

□

The MLNS estimate for the empirical trial distribution in Table XI is then found by implementing the maximisation routine in (B6) and is as shown in Table XII.

Appendix C: Vertex Enumeration

In this work we perform several vertex enumeration routines using the software **polymake** [51]. The first such task is that of enumerating the vertices of the three-party no-signalling polytope for binary settings and outcomes. The 48 no-signalling conditions in the linear relations expressed in (A1)- (A3) and the 8 normalisation conditions together constitute a set of hyperplanes, and the 64 non-negativity conditions constitute a set of closed half-spaces. The set of hyperplanes are the equality conditions expressible in a matrix format as $(\mathbf{H}_{\text{eq}})_{56 \times 64} \mathbf{P}_{64 \times 1} = \mathbf{b}_{56 \times 1}$, and the closed half-spaces are represented by the inequalities $(\mathbf{H}_{\text{ineq}})_{64 \times 64} \mathbf{P}_{64 \times 1} \geq \mathbf{0}_{64 \times 1}$. The no-signalling polytope Ξ_{ns} can then be represented as an intersection of finite number of closed half-spaces and hyperplanes as:

$$\Xi_{\text{ns}} := \{\mathbf{P} \in \mathbb{R}^{64} : \mathbf{H}_{\text{eq}} \mathbf{P} = \mathbf{b}, \mathbf{H}_{\text{ineq}} \mathbf{P} \geq \mathbf{0}\}. \quad (\text{C1})$$

Note that a subset of the total 48 no-signalling conditions is redundant, as these can be derived from a combination of normalisation conditions and the non-redundant no-signalling conditions. However, for the purpose of generating the vertices of Ξ_{ns} from its hyperplane representation using the **polymake** program, including these redundant no-signalling conditions does not pose any issue. There are 53856 vertices of the polytope Ξ_{ns} , and they can be classified into 46 equivalence classes [50].

Next, to approximate the set Δ_{lo2sr} with a polytope, we consider the intersection of Ξ_{ns} with the inequality in (1). Another polytope approximating Δ_{lo2sr} is the one obtained by the intersection of Ξ_{ns} with the inequality in (2). We can express both inequalities (1) and (2) as $\mathbf{B} \cdot \mathbf{P} \leq \beta$, where $\{B(abcxyz)\} =: \mathbf{B} \in \mathbb{R}^{64}$ is a Bell vector. As mentioned earlier in Section II, the Bell vector is not unique due to the no-signalling condition: the marginal correlators in the inequalities remain invariant under the settings choices of the party (or parties) not, so that a correlator such as for example $\mathcal{M}_{\text{AB}}^{00}$ can be represented multiple different ways as a linear combination of $P(abc|00z)$ terms using different choices of z . We express the inequalities in (1) and (2) as $\mathbf{B}_{(1)} \cdot \mathbf{P} \leq 4$ and $\mathbf{B}_{(2)} \cdot \mathbf{P} \leq 8$, where the Bell vectors $\mathbf{B}_{(1)}$ and $\mathbf{B}_{(2)}$ are as shown in tabulated form in Tables XIII and XIV. The sets $\Xi_{(1)} := \{\mathbf{P} \in \Xi_{\text{ns}} : \mathbf{B}_{(1)} \cdot \mathbf{P} \leq 4\}$ and $\Xi_{(2)} := \{\mathbf{P} \in \Xi_{\text{ns}} : \mathbf{B}_{(2)} \cdot \mathbf{P} \leq 8\}$ are the respective intersection of Ξ_{ns} with the closed half-spaces formed by the inequalities $\mathbf{B}_{(1)} \cdot \mathbf{P} \leq 4$ and $\mathbf{B}_{(2)} \cdot \mathbf{P} \leq 8$, and result in polytopes with 56767 and 57283 extreme points, respectively. The vertex enumeration routines that we perform in our work are summarised in Table XV. As mentioned in the main

TABLE XIII. Tabular representation of a Bell vector $\mathbf{B}_{(1)}$ corresponding to the inequality in (1).

		abc							
		000	001	010	011	100	101	110	111
xyz	000	3	-1	1	-3	-3	1	-1	3
	001	0	0	0	0	0	0	0	0
	010	1	1	-1	-1	-1	-1	1	1
	011	0	0	0	0	0	0	0	0
	100	0	0	0	0	0	0	0	0
	101	1	-1	-1	1	-1	1	1	-1
	110	0	0	0	0	0	0	0	0
	111	-1	1	1	-1	1	-1	-1	1

TABLE XIV. Tabular representation of a Bell vector $\mathbf{B}_{(2)}$ corresponding to the inequality in (2).

		abc							
		000	001	010	011	100	101	110	111
xyz	000	4	-4	4	-4	-4	4	-4	4
	001	1	1	-1	-1	-1	-1	1	1
	010	-1	1	1	-1	-1	1	1	-1
	011	-1	-1	1	1	1	1	-1	-1
	100	1	-1	-1	1	1	-1	-1	1
	101	2	-2	-2	2	-2	2	2	-2
	110	0	0	0	0	0	0	0	0
	111	2	-2	-2	2	-2	2	2	-2

text, the number of extreme points of the approximating polytopes correspond to the number of constraints in the respective test factor optimisation routines and, as explained earlier, we were able to reduce that number by restricting the optimisation feasibility region by requiring the condition $E[F] \leq 1$ for only those no-signalling behaviours that saturate the inequality intersecting Ξ_{ns} , which brings us to the vertex enumeration for the intersection of the no-signalling polytope with a Bell hyperplane: $\Xi'_{(1)} := \{\mathbf{P} \in \Xi_{\text{ns}} : \mathbf{B}_{(1)} \cdot \mathbf{P} = 4\}$ and $\Xi'_{(2)} := \{\mathbf{P} \in \Xi_{\text{ns}} : \mathbf{B}_{(2)} \cdot \mathbf{P} = 8\}$. The polytopes $\Xi'_{(1)}$ and $\Xi'_{(2)}$ have 3200 and 3664 extreme points, respectively. There are interesting features of the set $\text{Ext}(\Xi_{\text{ns}})$ with regards to the two linear witnesses. For instance, there is only one behaviour in $\text{Ext}(\Xi_{\text{ns}})$, denoted as $\mathbf{P}_{(1)}$ in (C2), that maximally violates $\mathbf{B}_{(1)} \cdot \mathbf{P} \leq 4$, achieving the value 6, and belongs to the equivalence class 8 (see Table 1 in [50]) of the extreme points of Ξ_{ns} . A relabelled version $\mathbf{P}_{(2)}$ of this behaviour (and hence belonging to the same equivalence class) maximally violates $\mathbf{B}_{(2)} \cdot \mathbf{P} \leq 8$ achieving the value 12.

$$\mathbf{P}_{(1)} := \begin{cases} P(0bc|0yz) = \frac{1}{4}\delta_{b,0}(\delta_{c,0} + \delta_{c,z}) \\ P(0bc|1yz) = \frac{1}{4}\delta_{b\oplus c,yz} \\ P(1bc|0yz) = \frac{1}{4}\delta_{b,1}(\delta_{c,1} + \delta_{c,z\oplus 1}) \\ P(1bc|1yz) = \frac{1}{4}\delta_{b\oplus c,yz\oplus z} \end{cases}, \quad \mathbf{P}_{(2)} := \begin{cases} P(0bc|0yz) = \frac{1}{4}\delta_{b,y}(\delta_{c,0} + \delta_{c,z}) \\ P(0bc|1yz) = \frac{1}{4}\delta_{b\oplus c,yz\oplus y} \\ P(1bc|0yz) = \frac{1}{4}\delta_{b,y\oplus 1}(\delta_{c,1} + \delta_{c,z\oplus 1}) \\ P(1bc|1yz) = \frac{1}{4}\delta_{b\oplus c,yz\oplus z\oplus y} \end{cases}, \quad \forall b, c, y, z \quad (\text{C2})$$

TABLE XV. Vertex Enumeration.

	Polytope	Number of Vertices	Remarks
(1)	Ξ_{ns}	53856	No-signalling polytope for (3,2,2) scenario
(2)	$\Xi'_{(1)} := \{\mathbf{P} \in \Xi_{ns} : \mathbf{B}_{(1)} \cdot \mathbf{P} = 4\}$	3200	Intersection of Ξ_{ns} and a hyperplane
(3)	$\Xi_{(1)} := \{\mathbf{P} \in \Xi_{ns} : \mathbf{B}_{(1)} \cdot \mathbf{P} \leq 4\}$	56767	Intersection of Ξ_{ns} and a closed half-space
(4)	$\Xi'_{(2)} := \{\mathbf{P} \in \Xi_{ns} : \mathbf{B}_{(2)} \cdot \mathbf{P} = 4\}$	3664	Intersection of Ξ_{ns} and a hyperplane
(5)	$\Xi_{(2)} := \{\mathbf{P} \in \Xi_{ns} : \mathbf{B}_{(2)} \cdot \mathbf{P} \leq 8\}$	57283	Intersection of Ξ_{ns} and a closed half-space

Table XVI categorises the candidates of the set $\text{Ext}(\Xi_{ns})$, which contains the extreme points of Ξ_{ns} , into various equivalence classes based on their saturation and violation of the two DI witnesses. For example, there are 8 entries from equivalence class 2, the “Popescu-Rohrlich (PR)” class of behaviours [50], that saturate equation (1), and 4 entries from the same class that saturate equation (2). Additionally, there are 32 entries from equivalence class 25, the “Guess Your Neighbour’s Input (GYNI)” class of behaviours [50], that saturate equation (1), and 24 entries from the same class that saturate equation (2). Interestingly, there are no entries from equivalence class 29 that saturate either equation (1) or equation (2), despite this class also being categorised as a GYNI class of behaviours [50]. However, equivalence class 29 does have 8 entries that violate equation (1) and 8 (possibly different) entries that violate equation (2). As demonstrated in Table XVI, there are numerous extreme points of Ξ_{ns} belonging to other equivalence classes that violate the DI witnesses in equations (1) and (2), and these classes were not explored in depth in [50].

TABLE XVI. Extreme points of Ξ_{ns} from the different equivalence classes described in [50] that saturate and violate the linear witnesses.

Eq. Class	# saturating (1)	# violating (1)	# saturating (2)	# violating (2)	Remarks
1	16	-	16	-	Local Deterministic Behaviours
2	8	-	4	-	Popescu-Rohrlich Behaviours
3	2	-	-	-	
5	8	-	8	-	
6	10	-	8	-	
8	8	1	8	1	
10	8	4	8	4	
12	20	4	16	8	
14	16	-	16	-	
15	-	16	8	16	
17	8	16	-	16	
18	16	-	8	-	
24	20	4	16	8	
25	32	-	24	-	GYNI Behaviours
26	16	-	16	-	
27	8	-	-	-	
28	16	-	16	-	
29	-	8	-	8	GYNI Behaviours
32	8	-	-	-	
40	4	-	-	-	
41	4	-	4	-	
42	8	-	8	-	

Appendix D: Another linear DI witness for genuine tripartite nonlocality

Here we prove that the inequality in (11) used as a DI witness in [30] is linear and hence can be expressed in the form $\mathbf{B} \cdot \mathbf{P} \leq \beta$. As mentioned in the main text, the inequality is a combination of two Bell games: (1) the CHSH game between parties A and B conditioned on C obtaining the outcome $c = 0$ for the measurement setting $z = 1$, expressed as

$$\text{CHSH}_{z=1}^{c=0} := \sum_{x,y} (-1)^{xy} \frac{\sum_{a,b} (-1)^{a \oplus b} P(ab0|xy1)}{\sum_{a,b} P(ab0|xy1)}, \quad (\text{D1})$$

and (2) the “Same” game, expressed as

$$\text{Same} := \mathcal{M}_{AB}^{02} + \mathcal{M}_{BC}^{20}. \quad (\text{D2})$$

The condition for perfect score for the **Same** expression requires all parties to obtain identical outcomes which can occur in one of two ways: both parties observe 0, or both parties observe 1. Violation of (11) serves as a DI witness for genuine tripartite nonlocality in the sense that the correlations are not achievable in a scenario where every set of two parties share a (possibly generalised) nonlocal resource and all parties have access to unlimited shared randomness. Here we show that it is a linear inequality by expressing it as:

$$\sum_{s,t=0}^1 [(-1)^{s \oplus t} \{P(st0|011) + P(st0|101) - P(st0|111) + 4P(sts|020)\} - 3^{s \oplus t} P(st0|001)] \leq 4. \quad (\text{D3})$$

We begin by writing the **Same** expression in (D2) as a weighted sum of probabilities using the linear relations in (A5) for the marginal correlators \mathcal{M}_{AB}^{02} and \mathcal{M}_{BC}^{20} , noting that no-signaling ensures that the expression for \mathcal{M}_{AB}^{02} (resp., \mathcal{M}_{BC}^{20}) is valid for any choice of third measurement z (resp., x):

$$\text{Same} = \sum_{a,b,c} (-1)^{a \oplus b} P(abc|020) + \sum_{a,b,c} (-1)^{b \oplus c} P(abc|020) \quad (\text{D4})$$

$$= 2(P(000|020) - P(010|020) - P(101|020) + P(111|020)) \quad (\text{D5})$$

$$= 2 \sum_{s,t} (-1)^{s \oplus t} P(sts|020). \quad (\text{D6})$$

The equality in (D5) results from expanding the two sums in (D4) followed by a cancellation of some terms. As an aside, notice that the **Same** expression achieves the perfect score of 2 if $P(a = b = c|020) = P(000|020) + P(111|020) = 1$, i.e., the parties should observe the same outcomes to achieve the perfect score.

Next, using the linear relation in (A5) for \mathcal{M}_C^1 and the normalisation condition that for any combination of settings the probabilities $P(abc|xyz)$ must sum (over the outcomes) to one, we can express the term $1 + \mathcal{M}_C^1$ appearing in the denominator of the second term on the left hand side of the inequality in (11) as:

$$1 + \mathcal{M}_C^1 = \sum_{a,b,c} P(abc|xy1) + \sum_{a,b,c} (-1)^c P(abc|xy1) = 2 \sum_{a,b} P(ab0|xy1). \quad (\text{D7})$$

The second equality in (D7) follows from expanding the two sums and a cancellation of some terms. Since by no-signalling (D7) holds for any combination of x, y , we choose $x = y = 0$. And then using the expression for $\text{CHSH}_{z=1}^{c=0}$ in (D1) we rewrite the left hand side of the inequality in (11) entirely in terms of the probabilities $P(abc|xyz)$ as shown below:

$$\text{CHSH}_{z=1}^{c=0} + \frac{4\text{Same} - 8}{1 + \mathcal{M}_C^1} = \sum_{x,y} (-1)^{xy} \frac{\sum_{a,b} (-1)^{a \oplus b} P(ab0|xy1)}{\sum_{a,b} P(ab0|xy1)} + \frac{4 \left(\sum_{s,t} (-1)^{s \oplus t} P(sts|020) - 1 \right)}{\sum_{a,b} P(ab0|001)} \quad (\text{D8})$$

Consider the first summation on the right hand side of the equality in (D8). The summand's denominator term $\sum_{a,b} P(ab0|xy1)$ is unchanged for any combination of x, y due to the no-signalling condition in (A4) that the composite system formed by parties **A** and **B** cannot signal to **C**. In other words, the outcomes observed by the party **C** are not influenced by the settings choices of the composite system (**A**, **B**). Hence, for $(x, y) \in \{(0, 1), (1, 0), (1, 1)\}$ we have:

$$\sum_{a,b} P(ab0|xy1) = \sum_{a,b} P(ab0|001), \quad (\text{D9})$$

using which we can rewrite the right hand side of (D8) as:

$$\sum_{x,y} (-1)^{xy} \frac{\sum_{a,b} (-1)^{a \oplus b} P(ab0|xy1)}{\sum_{a,b} P(ab0|001)} + \frac{4 \left(\sum_{s,t} (-1)^{s \oplus t} P(sts|020) - 1 \right)}{\sum_{a,b} P(ab0|001)}, \quad (\text{D10})$$

We then substitute the expression obtained above in the inequality in (11) and multiplying both sides by $\sum_{a,b} P(ab0|001)$ obtain:

$$\sum_{x,y} (-1)^{xy} \sum_{a,b} (-1)^{a \oplus b} P(ab0|xy1) + 4 \left(\sum_{s,t} (-1)^{s \oplus t} P(sts|020) - 1 \right) \leq 2 \sum_{a,b} P(ab0|001). \quad (\text{D11})$$

For the double summation on the left hand side of the above inequality, we expand the terms over all possible values of x, y , and then re-express the inequality as follows:

$$\sum_{a,b} ((-1)^{a \oplus b} - 2) P(ab0|001) + \sum_{a,b} (-1)^{a \oplus b} (P(ab0|011) + P(ab0|101) - P(ab0|111)) + 4 \sum_{s,t} (-1)^{s \oplus t} P(sts|020) \leq 4.$$

Notice that $\sum_{a,b} ((-1)^{a \oplus b} - 2) P(ab0|001) = -\sum_{a,b} 3^{a \oplus b} P(ab0|001)$. Now for the summations over binary variables a, b , one can instead choose to write them as summations over the binary variables s, t . The above inequality can then be re-expressed as (D3).